Overexpression, Purification, Spin-Labeling, and Characterization of Full-Length M2, an Integral Membrane Protein of Influenza A, in Detergent Micelles and in Mixed Lipid Vesicles

Honors Thesis in Chemistry

Richard Chen

Swarthmore College

May 27, 2013

Advisor: Professor Kathleen Howard

Abstract

M2 is a 97-residue, multi-functional transmembrane protein that has been implicated in processes important to viral replication, such as proton conduction and viral budding of Influenza A. Due to experimental difficulties associated with the overexpression of membrane proteins, previous structural studies of M2 have focused on various synthetic truncated forms of the protein, which has lead to incomplete and sometimes inconsistent results. Therefore structural studies of the full-length M2 protein avoid the potential artifacts associated with truncations and provide more physiologically relevant data regarding the M2 protein. This research describes the successful overexpression, purification, spin-labeling, and reconstitution of the full-length M2 into lipid vesicles. Circular dichroism (CD) spectroscopy and electron paramagnetic resonance (EPR) spectroscopy are also utilized to characterize the full-length M2 protein in both micelles and lipid vesicles.

Table of Contents

Chapter 1: M2's Role in the Influenza A Life Cycle

1.1 Influenza A: An Important Public Health Issue

Influenza A is the cause of the seasonal flu and is a public health threat. Infants and elderly are particularly vulnerable to infection. From the 2011-2012 influenza season, there are 26 laboratory-confirmed cases of influenza-associated pediatric death[1]. Particularly virulent strains of Influenza A had been the cause of multiple pandemics. The most recent pandemic was of the strain H1N1, "Swine Flu". By mid-March of 2010, estimated that about 59 million Americans contracted the H1N1 virus with 265,000 hospitalizations and 12,000 deaths[2]. Clearly, humans are at constant risk of being infected by the Influenza A, making research understanding and inhibiting the prophylaxis of Influenza A a particularly important endeavor.

The Influenza A virus is a negative stranded RNA virus[3]. Influenza A contains three different surface proteins. In high abundance are spike glycoproteins, neuraminidase (NA) and Hemagluttinin (HA) (Figure 1.1. blue and red). Expressed in low numbers relative to HA and NA is matrix protein 2 (M2) (Figure 1.1 purple). Additionally, the virus possesses a lipid envelope, taking shape as either a sphere or a tubule, and the shape of the virus largely depends on the identity of the infected host cell[3,4]. Influenza A virus contains eight strands of RNA bound to nucleopaside proteins (RNPs) that encode 11 proteins, a few of which are HA, NA, M2, and matrix protein 1 (M1)[3].

The virus enters the host cell via receptor-mediated endocytosis. The virus is targeted to host cells by HA, which binds to the sialic acid present on the cell surface of

the host. Following receptor-mediated endocytosis, the acidification of the virion-containing endosome to pH 5-6 enables uncoating and subsequent release of the viral RNPs into the cytoplasm of the host cell. The transcriptionally active viral RNPs are then delivered to the host nucleus, enabling the reproduction of the virus genome[5]. Lastly, enzymatic cleavage of HA by NA enables the release of progeny virions[3].

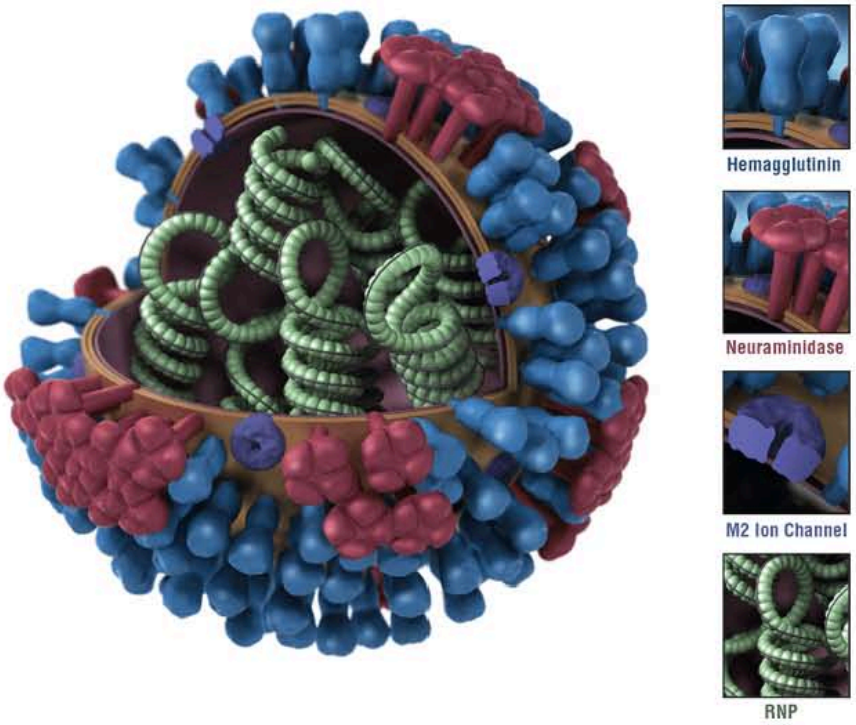

Figure 1.1. Cartoon of Influenza A with surface proteins of viral envelope. Shown are Hemagluttinin (HA) (blue), neuraminidase (NA) (red), M2 (purple), and RNA-bound nucleocapsides (RNP) (green). Figure adapted from[6].

1.2 Roles of M2 in the Viral Life Cycle

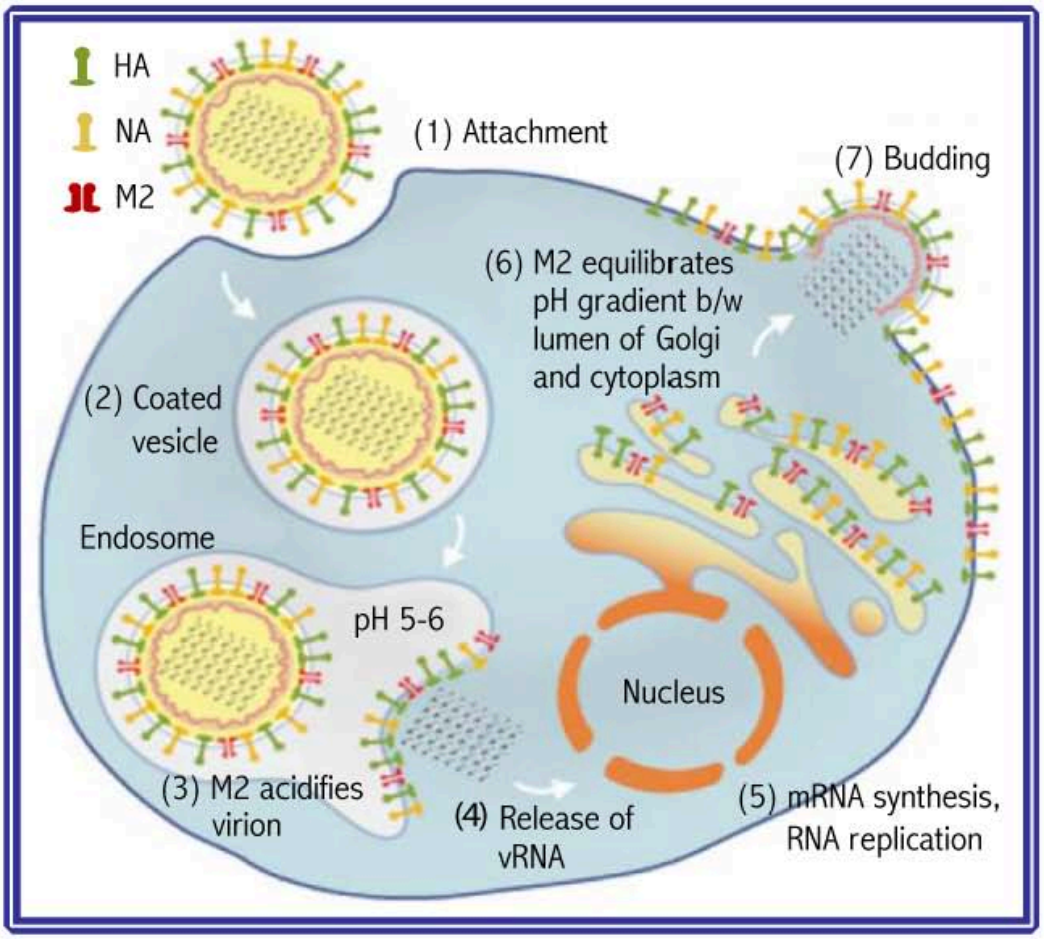

Figure 1.2. Role of M2 in the Influenza A life cycle. (3) M2 acidifies the virion, enabling the release of viral genetic material. (6) M2 equilibrates the pH between the lumen of Golgi and cytoplasm and (7) facilitates viral budding. Figure adapted from[7].

Steps (3) and (6) demonstrates that the proton channel function of M2 is essential for viral replication (Figure 1.2). Following entry of the virion into the host cell via receptor-mediated endocytosis, the clatherin-coated vesicle dissociated to form a mildly acidic endosome. As the endosome matures into a lysosome, its internal pH is lowered to pH 5-6, and M2 is activated to allow protons to enter the viral interior[7]. The activation of M2 causes dissociation of viral RNPs from M1[8]. Once viral RNPs are released into the host cell cytoplasm, they are transported to the cell nucleus, enabling transcription and replication of the viral genome. Step (6) demonstrates that M2 is also important in

equilibrating the pH gradient between the lumen of the Golgi and the cytoplasm, which prevents the misfolding of pH-sensitive HA[9]. Studies involving site-directed mutagenesis of M2 have shown that His 37 and Trp 41 are important in proton transport. The imidazole side chain of His serves as a pH sensor, allowing protons to be selectively conducted across the channel. The indole ring of Trp 41 forms a gate for the channel pore[8].

M2 has also been demonstrated to be important in viral budding. The budding function of M2 is largely uncharacterized. However, it has been proposed that the binding of cholesterol through the amphipathic helix of the C-terminal region leads to a negative membrane curvature in the cholesterol-containing vesicles[10, 11]. Further information on the role of cholesterol and M2 in viral budding is discussed in section 1.3.

1.3 Overview of Structure and Function of Three Domains of M2

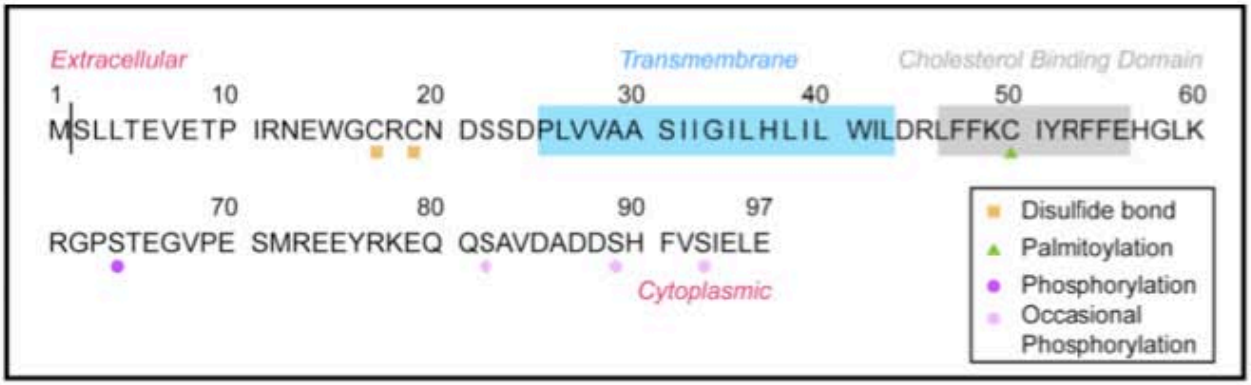

Figure 1.3. Primary sequence of the M2 protein A/Udom/H3N2 strain showing three distinct domains. The N-terminal domain is located in the extracellular region, and the C-terminal tail is located in the cytoplasm.

M2 is a homotetramer, comprising of 97 amino acid residues. M2 consists of a 24-residue N-terminal extracellular domain, a 19-residue transmembrane (TM) domain, and a 54-residue cytoplasmic tail. Kochendoerfer and colleagues previously synthesized full-length M2 by separately synthesizing and ligating two segments of M2[12]. Analytical

ultracentrifugation of the full-length peptide showed that M2 persisted predominantly as tetramers. Furthermore, partial digestion of the full-length with trypsin and chymotrypsin revealed a highly structured region spanning 15-20 residues immediately C-terminal to the TM domain. Additionally, circular dichroism (CD) spectroscopy of M2 in 1-palmitoyl-2-oleoyl-sn-glycero-3-phosphocholine (POPC) and dodecylphosphocholine (DPC) micelles showed the presence of a significant alpha-helical structure. Moreover, CD spectroscopy of M2 reconstituted in DPC revealed that as many as 40 residues that had alpha helical secondary structure. The combined results revealed that M2 assembled natively into a tetramer with each subunit containing an unstructured N-terminal extracellular domain, a TM helix, a highly structured alpha helical region spanning 15-20 residues immediately C-terminal to the TM helix, and a disordered cytoplasmic tail.

The TM region, which forms the pore of the ion channel had been established to be essential for proton conduction and binding of amantadine. Leiding and colleagues' electrophysiological studies compared proton conduction of full-length M2 and the M2TM construct (residue 22-46) and demonstrated that the TM region of M2 was essential for proton conduction[13]. Further, inhibition of proton conduction in full-length M2 was found to be comparable to that of the M2TM construct, which confirmed the structural data that showed that the transmembrane region of M2 as the binding site for amantadine[14].

Studies of full-length M2 proteins with mutations disrupting highly-conserved amphipathic helix within the cytoplasmic tail showed that the amphipathic helix was important for facilitating viral budding[3]. Analysis of the amino acid sequence of M2 across all influenza subtypes of 500 different strains of Influenza A virus revealed a

highly conserved amphipathic helix spanning 17 amino acid residues[3]. Rossman and colleagues conducted electron microscopy studies on both the full-length wild-type M2 (WT-M2) protein and the full-length M2(AH-Mut) mutant protein reconstituted in giant unilamellar vesicles (GUVs) that were constructed using 1,2-dioleoyl-sn-glycero-3-phosphocholine (DOPC), saturated sphingomyelin (SM) and cholesterol. The M2(AH-Mut) protein was generated by altering the hydrophobic face of the amphipathic helix via changing five bulky hydrophobic residues to Ala, so to retain the alpha-helical structure of the amphipathic helix. Rossman and colleagues found no evidence of budding with M2(AH-Mut) protein reconstituted in GUVs. However, the researchers observed budding, as evidenced in the formation of many intra-luminal vesicles (ILVs) in the WT-M2 protein reconstituted in GUVs, which suggested that the amphipathic helix is essential for viral budding.

Finally, the unstructured N-terminal ectodomain (residues 1-24) was found to be important for M2's incorporation into the virion[15]. It was observed that the amino acid sequence of the N-terminal ectodomain was highly conserved across multiple strains of Influenza A, which had been a target of interest for vaccines[16]. Consequently, elucidating the structure and mechanism of action of the N-terminal ectodomain is thought to potentially lead to new anti-flu drugs, which would combat Influenza A's increasing resistance to existing anti-flu drugs[15].

1.3 Are There Discrepancies in Structural Data that Arise from Study of Truncations?

Until recently, the majority of biophysical and structural studies of M2 have employed the usage of synthetic truncations. In the absence of tractable recombinant

DNA-based expression methods, chemical synthesis has been utilized in order to produce large quantities of M2 needed for structural studies[12]. However, prevalent aggregation of the highly hydrophobic regions of the shorter M2 peptides and difficulties associated with solubilizing the hydrophobic segments during peptide synthesis prevent the viable total synthesis of the full-length protein[17]. To date, the only attempt at the total synthesis of full-length M2, which has been done by chemical ligation of two synthesized M2 segments, reports 18% overall yield after purification[12].

In the absence of viable methods for obtaining large quantities of full-length M2, structural studies have employed the usage of truncations with wide variability in the truncations studied. Current structural studies of M2 show divergent high-resolution structures, which can either be attributed to structures of different important conformations of M2 or can be attributed to experimental artifact potentially due to use of different synthetic truncations (Figure 1.4). While the structures of the transmembrane region are in close agreement, the structure of C-terminal amphipathic helix differ. On one hand, the structure of residues 18-60, published by Schnell and Chou, shows the cytoplasmic helix forming a tetrameric bundle that extends into the cytoplasm beyond the end of the transmembrane domain[18]. On the other hand, the structure of residues 22-62 published by Cross, et. al places the cytoplasmic helix at the C-terminal end of the bundle near the headgroup region of the bilayer[19] (Figure 1.4 (a)). The high-resolution structure by Cross, et. al, however, seems more consistent with the viral budding function of M2, as the C-terminal helix is properly positioned to interact with cholesterol in the membrane bilayer[10].

The difference in truncations used in these studies points to the possibility that the specific truncations influence the protein conformations are accessed, and small differences in the sequence of truncations can lead to large changes in observed structure. While the relative importance of the two high-resolution structures in terms of the region C-terminal to the transmembrane region is up to speculation, the structural studies of the full-length M2 can potentially provide such answers.

In recent years, the study of full-length M2 has become more tractable, as protocol for over-expressing and purifying M2 has been published[13]. Thus, studies of full-length M2 should provide more physiologically relevant data. This research seeks to characterize the full-length M2 and to provide methods that enable its structural determination.

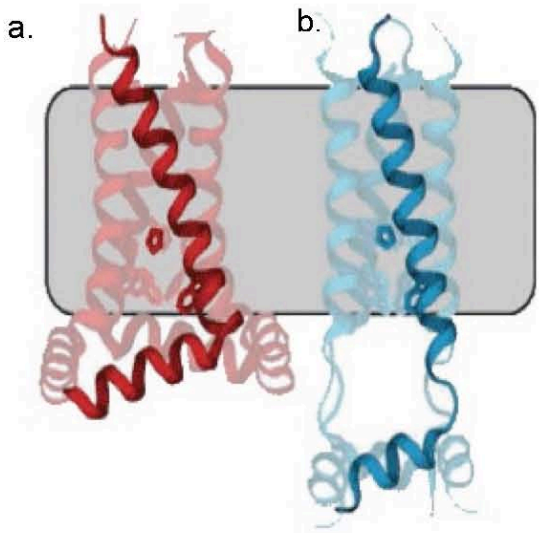

Figure 1.4. High resolution structures of M2 (a) Cross, et al. solid-state NMR structure of residues 22-62 (PDB: 2L0J) and (b) Schnell and Chou solution NMR structure of residues 18-60 (PDB: 2RLF).

Chapter 2: Expression and Purification of M2FL

2.1 Overexpression of M2FL

Frozen *Escherichia coli* cultures that were transformed with pET23D(+) plasmids containing modified, full-length M2 genes were obtained from the DeGrado group[13] (Sequence available in Appendix I). One M2 sequence, designated which we call M2FL-WTe, was modified from the wild-type Udorn strain (GenBank accession no. CAD22815) and possessed four extra mutations (W15F, C17S, C19S, and C50S) and a C-terminal His-tag. Point mutations and His tag were added in order to simplify the purification process and to improve the purification yield (Figure 2.1). The other M2 sequence, designated M2FL-C19, possessed the same modification as M2FL-WTe but retained its natural C19 (Figure 2.1). Electrophysiology studies on M2FL-WTe reconstituted in large unilamellar vesicles showed that the selectivity and rate of proton conduction for M2FL-WTe is similar to those found in those expressed in whole cells[13, 20].

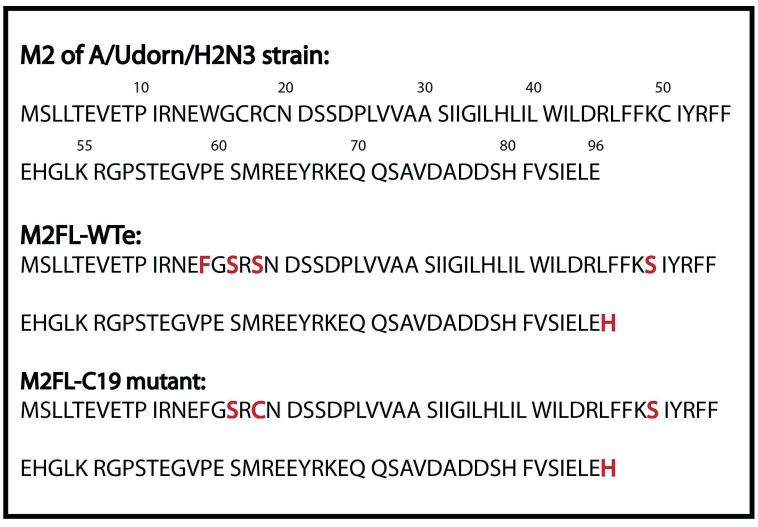

Figure 2.1. Sequence of the full-length M2 of A/Udorn/H2N3 strain and sequences of modified full-length constructs that were overexpressed in *E. coli.* Bolded sites in red highlight the changes from the wild-type strain.

Our expression protocol followed the one used by Leiding, et. al with modification made to purification to adopt to instrumentation available at Swarthmore College. Glycerol stocks containing transformed *E. Coli* cells were streaked on LB agar plates containing 100 μg/mL of ampicillin and incubated overnight at 37 °C. After incubation, a single colony was transferred from the ampicillin LB agar plates to 5 mL of LB broth solution supplemented 100 μg/mL ampicillin and incubated for eight hours at 37 °C. 0.5 mL of the liquid culture was then diluted with 50 mLs of LB broth solution supplemented with 100 μg/mL ampicillin and was shaken overnight at 200 rpm in 37 °C. Following the overnight incubation, the 50 mL of liquid culture was transferred to 1 L of LB solution containing 100 μg/mL ampicillin and shaken at 200 rpm in 37 °C. The growth of *E. Coli* in the 1 L LB medium was charted by monitoring the liquid culture's absorbance at 600 nm (OD_{600}). When OD_{600} of the liquid culture reached 0.7-1.0, M2 overexpression was induced with 1 mM isopropyl β-D-1-thiogalactopyranoside (IPTG). Overexpression of M2 by E. coli was allowed to proceed by shaking the liquid culture at 200 rpm in 37 °C for three additional hours. M2 overexpression was halted by pelleting the cells at 4000 rpm at 4 °C for 30 min. The excess supernatant was discarded and the cells were resuspended in 50 mL Falcon tubes using the remaining LB. The resuspended cells were then pelleted again at 4000 rpm at 4°C for 30 min and the remaining LB was discarded. Pelleted cells were then stored at -80°C prior to lysis and M2 purification.

2.2 Lysis of M2-overexpressing cells by bath sonication

Frozen cells were first resuspended in lysis buffer consisting of 50 mM Tris, 40 mM OG, 150 mM NaCl, 0.2 μg/mL DNase I, 500 μM 4- benzenesulfonyl fluoride hydrochloride (AEBSF), and 25 μg/mL lysozyme (~ 1 L of growth/50 mL of lysis

buffer). Visible chunks found in liquid culture were completely dissolved by 40 alternating cycles of end-over-end inversions and 15 sec bath sonication in a bath-type ultrasonic disintegrator designed for liposome preparation (G112SP1 Special Ultrasonic Cleaner, Laboratory Supplies Company, Hicksville, NY). The lysis procedure using a bath-type ultrasonic disintegrator was optimized by comparing the viscosity and the overall protein yield of the resulting lysate at various lysis cycles (results not shown). Following the cell lysis, cellular debris and solubilized M2FL protein were separated by centrifugation at 16,000 rpm at 4 °C.

2.3 Ni-Affinity Chromatography of Lysate

The detergent-solubilized M2FL protein, present in the supernatant, was separated from the pellet and was further purified by Ni-NTA column chromatography. The 20 mL of supernatant was initially incubated with 3-4 mL of Ni-NTA super-flow resin (Qiagen) and 20 mM imidazole at 4 °C for 30 min with gentle shaking. M2-bound resin was then sequentially washed with three washing buffers, designated Wash 1-3, containing increasing concentrations of imidazole and decreasing concentrations of OG detergent and NaCl[13]. (Wash 1: 50 mM Tris (pH 8), 150 mM NaCl, 40 mM OG, 20% v/v glycerol; Wash 2: 50 mM Tris (pH 8), 20 mM OG, 20% v/v glycerol; Wash 3: 50 mM Tris (pH 8), 4 mM OG, 20% v/v glycerol, 20 mM imidazole). Finally, the His-tagged M2 protein was eluted and stored in buffer consisting of 50 mM Tris (pH 8), 4 mM OG, 20% v/v glycerol, and 300 mM imidazole at -4 °C (Figure 2.2).

E. coli lysate, three continuous wash steps with increasing imidazole (wash 1-3), Ni-NTA column eluant and the RP-HPLC product were sampled for M2FL-WTe. Samples were subsequently stained with Coomassie Brilliant Blue R-250 (CBB) with

reducing buffer and were analyzed via electrophoresis on a 15% acrylamide SDS-PAGE gel.

SDS-PAGE gel electrophoresis of each step of purification for M2FL-WTe suggested that the purified product is highly pure (Figure 2.2). Washes 1-3 (W1-W3) displayed the elimination of impure species while retaining the His-tagged protein. Moreover, in comparison to the lysate and Ni-NTA column flow-through (lanes 1-2), both the Ni-NTA eluted and the RP-HPLC proteins displayed fewer bands, which further demonstrated the elimination of impure species that there were concurrently present in the lysate.

The band corresponding to the purified M2FL on the SDS-PAGE gel had a mobility between the 10 and 15 kDa protein standards, which is in agreement with the calculated mass of the monomer of M2FL-WTe, which is 11,892 Da (Figure 2.2). Formation of dimers or tetramers was not significant in the E lane on the SDS-PAGE gel. At high concentrations of RP-HPLC M2FL-WTe, the protein showed discrete high molecular weight bands, suggesting the formation dimers, tetramers, and higher order species (Figure 2.2, $[RP]_H$). Notably, though, at low concentrations of RP-HPLC M2FL-WTe (Figure 2.2, $[RP]_L$), the oligomerization of M2FL was not observed.

While prior work done by the DeGrado group implemented RP-HPLC to purify M2FL[13], RP-HPLC was not implemented for spin-labeled M2FL (Chapter 4) to avoid potential degradation due to HPLC methods and because sufficient purity was obtained via Ni-affinity chromatography (Figure 2.2).

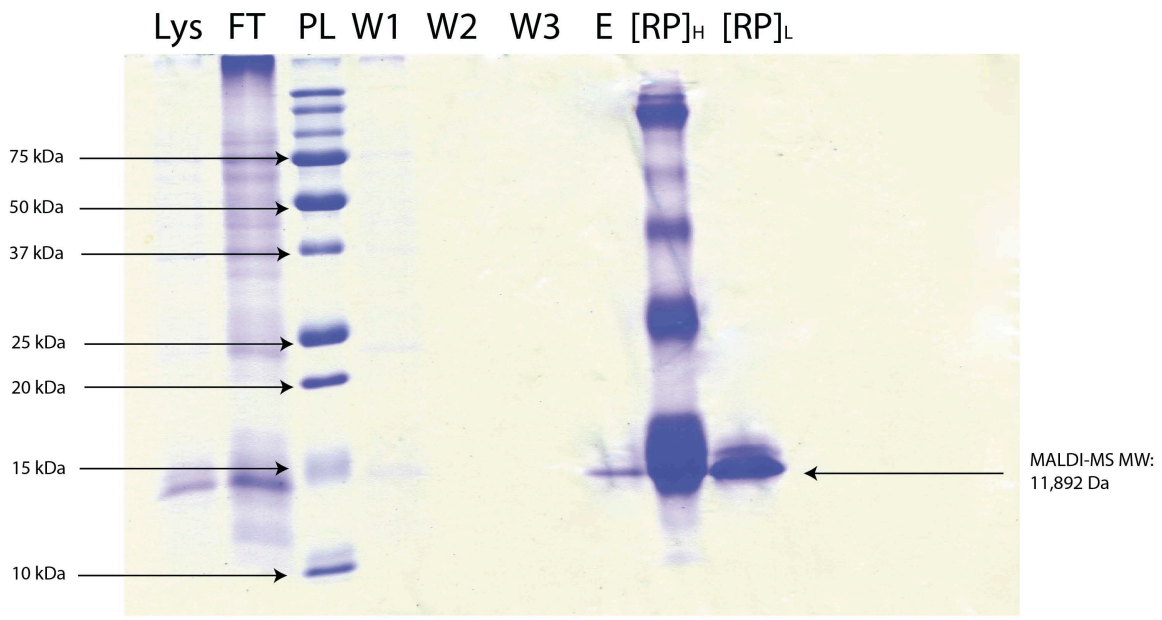

Figure 2.2. 15% acrylamide SDS-PAGE electrophoresis of M2FL-WTe purification. Steps of M2FL-WTe purification is displayed sequentially from left to right: 1) Lysate; 2) FT: Ni-NTA column flow-through; 3) PL: 10-250 kDa Protein Ladder; 4) W1: 50 mM Tris (pH 8), 50 mM NaCl, 40 mM OG, 20% v/v glycerol; 5) W2: 50 mM Tris (pH 8), 50 mM NaCl, 20 mM OG, 20% v/v glycerol; 6) W3: 50 mM Tris (pH 8), 4 mM OG, 20% v/v glycerol, 20 mM imidazole; 7) E: Eluted protein from the Ni-NTA column; 8) $[RP]_H$: Highly concentrated RP-HPLC purified product; 9) $[RP]_L$: Dilute RP-HPLC purified product.

2.4 Reverse-phase HPLC Purification of M2FL-WTe

Reverse-phase high performance liquid chromatography (RP-HPLC) was conducted on the protein-containing Ni-NTA column eluant for further purification and to eliminate the highly concentrated imidazole background. M2FL-WTe was purified on Vydac C_4 columns (Hesperia, CA) that were connected to a Waters 1525 Binary HPLC Pump (Milford, MA). The columns were packed with reversed-phase material consisting of butyl aliphatic groups bonded to the surface of silica with large pores (300 Å diameter). Separation was achieved using a gradient of solvent A (0.1% TFA in H_2O) and solvent IB (60% isopropanol + 30% acetylnitrile, 10% water, 0.1% TFA). Elution of the protein was monitored with a Waters 2487 Dual Wavelength Absorbance Detected

Set at 280 nm and 220 nm, which corresponded to the absorbance of Trp residues and the peptide backbone, respectively.

RP-HPLC purification of M2FL-WTe was performed on a Preparative Column (Vydac Catalog #214TP1022, 10 μm particle diameter, 22 mm internal diameter x 25 cm). HPLC optimization was conducted by monitoring the elution of M2 under three different linear gradient of solvent IB versus solvent A (Figure 2.3). For all solvent gradients, the elimination of the high imidazole buffer occurred between 9 and 15 mins. However, further separation of the protein peak with a retention time centered at 17 mins was observed (Figure 2.3a). Decreasing the solvent gradient resulted in the increase in solvent polarity, which corresponded in increased retention time of the protein. As the solvent gradient was decreased from a linear gradient of solvent IB versus solvent A of 50-100% in 30 mins (Figure 2.3a) to 50-80% in 30 mins (Figure 2.3b), a right shoulder corresponding to a protein species with a higher MW appeared. Its similar elution time relative to that of M2FL-WTe suggested that this protein possessed similar hydrophobicity and size in comparison to M2FL-WTe. Solvent gradient was lowered further to 50-70% solvent IB versus solvent A in 30 mins in attempt to isolate and characterize the higher MW species (Figure 2.3c). Despite the fact that the two protein peaks were poorly resolved, an attempt was made to collect the two species in separate aliquots for further analysis.

The absorbance peak with retention time centered at ~18 mins, which corresponded to the elution of M2FL-WTe was collected in separate aliquots from the right shoulder component with retention time centered at ~20 mins. The eluted fractions of the M2FL-WTe were then reduced to half of its original volume under a gentle stream

of N_2 gas. The evaporated organic solvent was then replaced with an equal volume of H_2O to facilitate freeze-drying. After lyophilizing M2FL-WTe, the protein was then stored at -20 °C for future use.

The SDS-PAGE electrophoresis gel of M2FL-WTe purification suggested that protein purification with a Ni-NTA column was sufficient (Figure 2.2). Such conclusion was supported by the observation that one protein peak observed on the RP-HPLC for both M2FL-WTe which indicated the absence of other protein species. Consequently, future protein purifications did not include purification via RP-HPLC, so to reduce purification time and possible degradation due to HPLC methods.

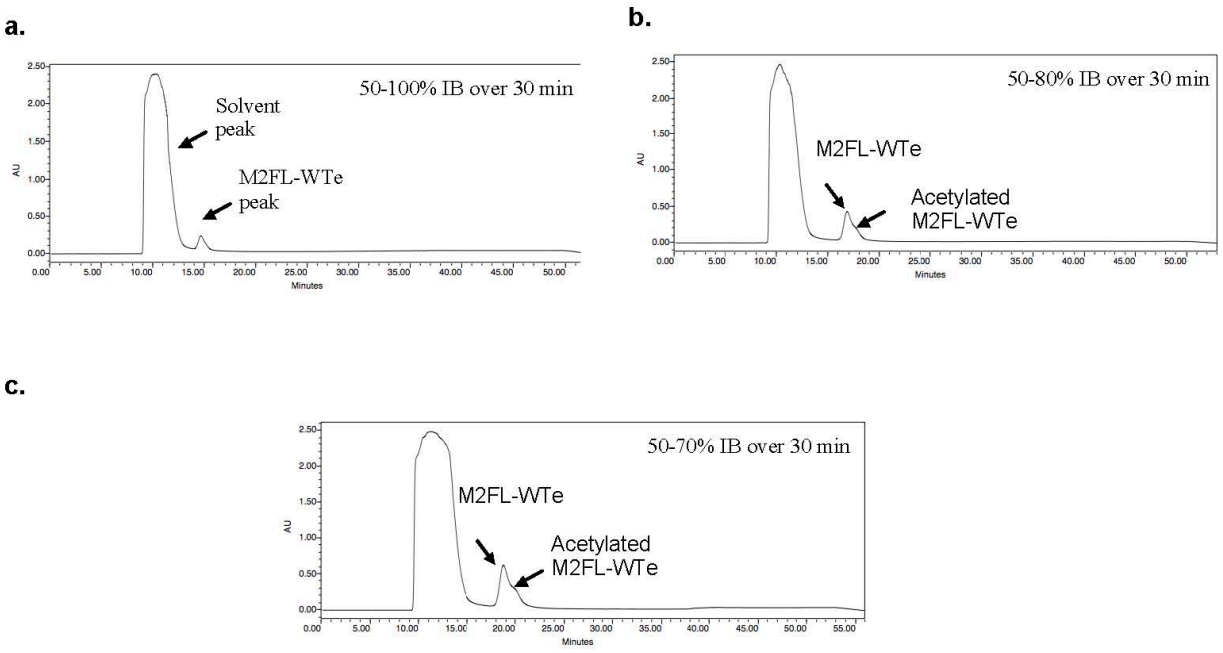

Figure 2.3. Representative RP-HPLC chromatographs. Purification of M2FL-WTe with a linear gradient of solvent IB versus solvent A of (a) 50-100% 30 min, (b) 50-80% in 30, (c) 50-70% in 30 min. Elution of M2 was monitored at 280 nm.

2.5 MALDI-Mass Spectrometry of M2FL

Matrix-assisted laser desorption/ionization (MALDI) mass spectrometry was conducted on the lyophilized form of the eluted protein species. The resulting mass spectra revealed the presence of two species, corresponding to the M2FL-WTe and an acetylated form of M2FL-WTe (mass spectrum not shown). The major peak corresponded to a mass of 11,892 Da, which matched the mass of M2FL-WTe calculated from the primary sequence. The minor +40 Da peak corresponded to the shoulder observed in the HPLC trace, and the +40 Da molecular weight was associated with a post-translational N-terminal acetylation [13].

2.6 Overall Overexpression Yields

The expression and purification yields of M2FL-WTe was 30 mg/L of growth. The yield for M2FL-WTe was lower compared that obtained Leiding and colleagues, which was 55 mg/L of growth[13]. The lower yield was expected due to the decision to exclude the acetylated form of M2FL-WTe, which was included as total yield of M2FL-WTe by Leiding. Furthermore, lower yields were potentially a consequence of reduced efficiency of cell lysis by using a lower-powered bath sonicator compared to a high-powered tip sonicator that was used[13]. As cell lysis was reduced, less of the overexpressed protein becomes accessible to extraction and would then be discarded along with the cellular debris during a step of the purification process. Nevertheless, the utilized expression and purification protocol still yielded a sufficient amount of protein for EPR studies which required ~30 μg of protein per sample. In the future, Howard lab

will pursue the use of a tip sonicator to further improve the efficiency of lysis and full-length M2 extraction.

Chapter 3: Characterization of Wild Type Full-Length M2 (M2FL-WTe)

3.1 Characterization of M2FL-WTe via UV-Vis Spectroscopy

UV-Vis spectrum of M2FL-WTe in TFE is compared to those of M2TM WT and M2TMC truncations (Figure 3.1). The UV-Vis spectra were recorded from 340 to 200 nm on a Varian Cary 50 UV-Vis spectrophotometer with a scan rate of 300 nm/min and a data interval of 0.5 nm. Above 275 nm, the absorbance of M2 peptides can be estimated by the contribution of three chromophores: the aromatic residues Trp, Tyr, and disulfide bonds (Cystine)[21]. M2's molar absorptivity coefficient at 280 nm, ε_{280}, in TFE is estimated by the contribution of the molar absorptivity coefficients via the following equation:

$$\varepsilon_{\lambda M2} = \#_{Trp}(\varepsilon_{Trp}) + \#_{Tyr}(\varepsilon_{Tyr}) + \#_{S-S}(\varepsilon_{S-S}) \quad (1)$$

Table 3.1 lists the numbers and identity of chromophores corresponding to M2TM (residues 22-46), M2TMC (residues 23-60), and M2FL-WTe as well as the molar absorptivity coefficients of model chromophores, (Trp, Tyr, Cystine) in propanol. Based on equation (1) and data presented in Table 3.1, the molar absorptivity coefficients of various M2 constructs in TFE can be reasonably estimated, as the dielectric constant of TFE is much closer to that of propanol compared than to that of water (D_{TFE} = 27.7, $D_{1\text{-}propanol}$ = 20.1, D_{Water} = 80.1 at 20 °C). From Table 3.1, it can be seen that M2FL-WTe possesses the highest chromophore content and, consequently, the highest molar absorptivity coefficient compared to M2TM and M2TMC truncations.

Furthermore, differences in UV-Vis spectra between the three M2 constructs are reflective of their primary sequences. It can be seen on Figure 3.1 M2FL-WTe share similar absorbance spectrum character relative to M2TMC near 285-260 nm and 265-245

nm, which correspond to absorbance of their Phe and Tyr residues, respectively. Since M2TM does not possess any Phe or Tyr residue, its UV-Vis spectrum at regions near 285-260 nm and 265-245 nm shows the absence of absorbance due to Phe and Tyr residues, resulting in a significantly different absorbance spectrum compared to M2FL-WTe and M2TMC.

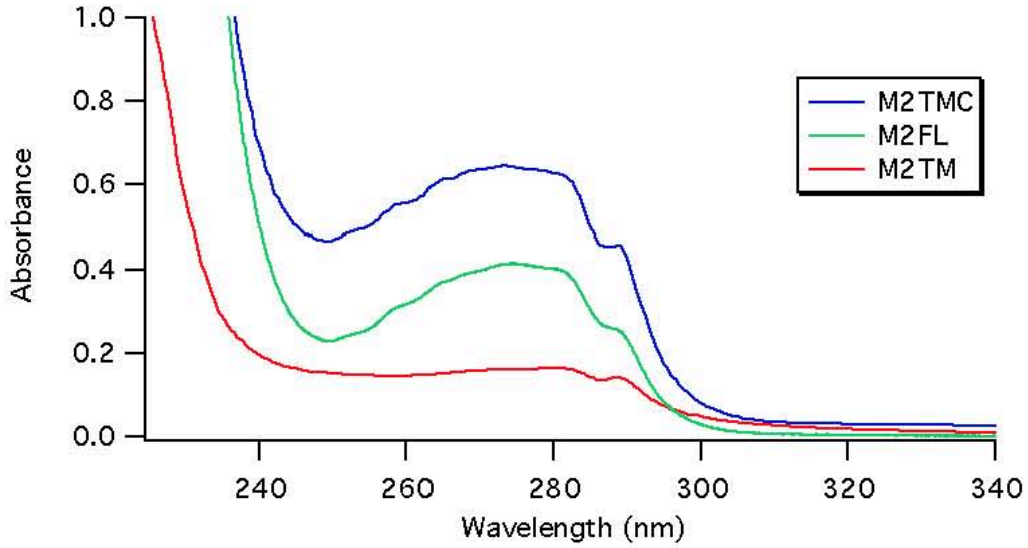

Figure 3.1. UV-Vis spectra of M2TM, M2TMC, and M2FL in TFE.

Table 3.1. Comparison of the molar absorptivity coefficients of M2 truncations and M2FL-WTe in TFE at 280 nm

	Trp model	Tyr model	Cystine (S-S) model
ε_{280} in propanol (M^{-1} cm^{-1})	6,075	1,680	135

Peptide/Protein	Chromophore content	Estimated ε_{280} in TFE (M^{-1} cm^{-1})
M2TM (22-46)	1 Trp	6,075
M2TMC (23-60)	1 Trp + 1 Tyr	7,755
M2FL-WTe expressed*	1 Trp + 2 Tyr	9,435

*sequence shown in Figure 2.1

3.2 Characterization of M2FL-WTe in Detergent Micelles

Circular dichroism (CD) spectroscopy of proteins can provide information about secondary structure. The α-helical secondary structure of aqueous-soluble proteins has been well characterized to exhibit distinctive CD absorbance. The α-helical peptide backbone interacts distinctively with circularly polarized light compared to β-sheets and unstructured peptides[22,23]. Specifically, alpha helices exhibit strong, negative absorbance at 208 and 222 nm. M2TM, M2TMC, and a synthetic full-length construct have been shown to possess a significant α-helical character secondary structure in detergent micelles[12]. The spectral shape analysis of the synthetic full-length construct, estimates that at least 45 residues are α-helical in character compared to the estimated 16 α-helical residues in M2TM[12].

The energy transitions associated with the peptide backbone are observable at near-UV wavelengths. However, detergent micelles cause significant scattering of low-wavelength regions[22]. Furthermore, circularly polarized light undergoes differential scattering in presence of micelles[22]. Consequently, CD spectroscopy of M2FL in detergent micelles is challenging due to scattering effects. To investigate the extent of scattering and to provide a comparison of CD spectrum, the CD spectrum of the aqueous soluble equine-skeletal myoglobin (Mb) (Sigma-Aldrich) in presence of detergent micelles was also obtained. Mb has been selected because it possesses high degree of α-helical secondary structure and is expected to remain folded in presence of detergent micelles. The resulting CD spectrum of Mb, therefore, can inform the extent of light scattering due to presence of detergent micelles.

CD measurements were made using an Aviv 720 circular dichrometer at 25 °C. The CD spectra were recorded from three average stepwise scans from 260 to 198 nm with averaging time of 0.3333 seconds using a 1 mm quartz cell. Either lyophilized M2FL or lyophilized equine-skeletal myoglobin (Mb) was added to 10 μM n-dodecylphosphocholine (DPC) detergent (Avanti Polar Lipids) micelles dissolved in aqueous buffer consisting of 50 mM Tris (pH 7.8), 100 mM KCl[12] (Figure 3.2). Baselines were recorded and subtracted after each spectrum.

Table 3.2. Properties of n-octyl-β-D-glucoside (OG) and n-dodecylphosphocholine (DPC). (Information about OG and DPC are adapted from www.piercenet.com and www.avantilipids.com)

Name	Chemical formula	Length of Fatty Acid Chain	Critical Micelle Concentration (CMC) (mM)
n-octyl-β-D-glucoside (OG)	$C_{14}H_{28}O_6$	8	23-25
n-dodecylphosphocholine (DPC)	$C_{17}H_{38}NO_4P$	12	1.1

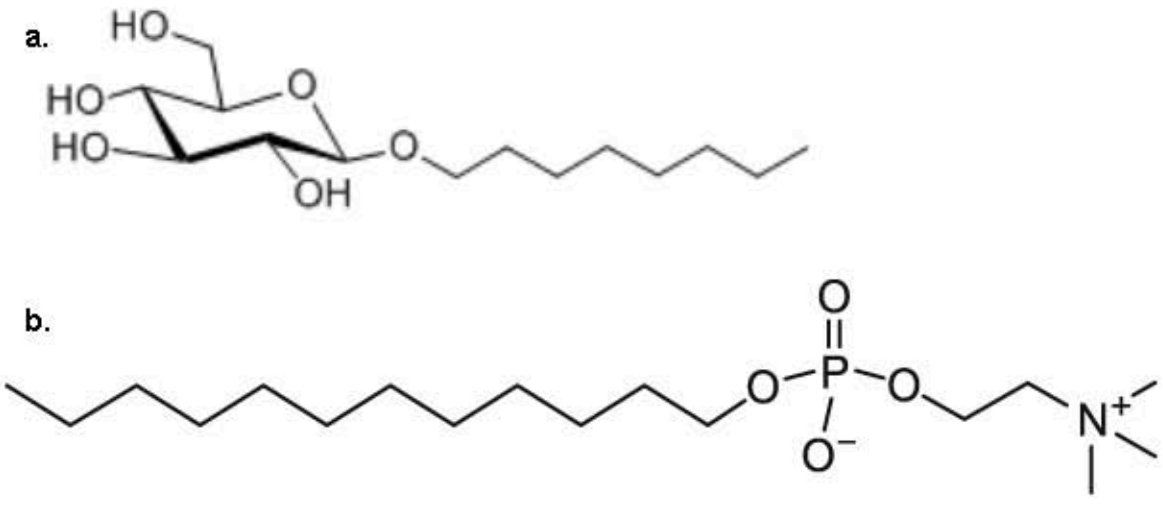

Figure 3.2. Chemical structure of (a) n-octyl-β-D-glucoside (OG) and (b) n-dodecylphosphocholine (DPC).

The presence of negative bands at 209 and 223 nm in the CD spectra of Mb in either aqueous buffer or in presence of detergent micelles verified that the secondary structure of the protein was predominantly alpha-helical (Figure 3.3). However, both CD spectra of Mb showed that the expected strong, positive peak at 190 nm was significantly distorted, which suggested that scattering effects were highly significantly at wavelengths < 200 nm. Nevertheless, the presence of negative bands at 209 and 223 nm was sufficient in confirming the presence of alpha-helical secondary structure. Future CD measurements excluded absorbance data at <200 nm.

M2FL was then reconstituted in either n-octyl-β-D-glucoside (OG) (Avanti Polar Lipids) or DPC near their respective critical micelle concentrations (Table 3.2). OG and DPC detergents were selected because M2FL was solubilized in OG after purification, and DPC detergent was commonly used as a reconstitution medium for CD studies of M2[12,24,25].

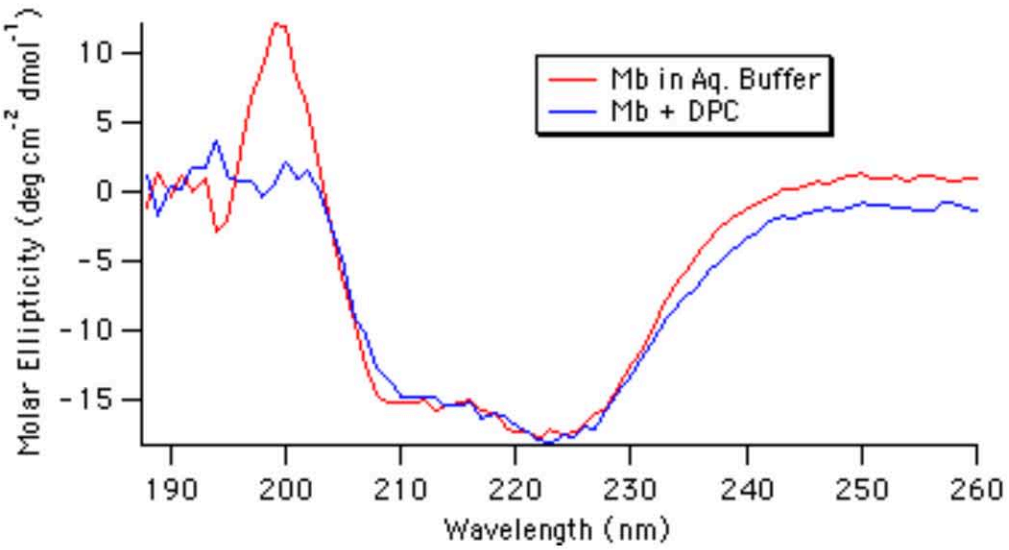

Figure 3.3. CD spectra of equine skeletal myoglobin in aqueous buffer consisting of 50 mM Tris (pH 7.8), 200 mM KCl (red) and in presence of 10 μM DPC micelles (blue).

Samples were created such that their final concentrations consisted of 50 μM M2FL in 50 mM Tris (pH 7.8), 200 mM KCl with either 25 mM OG or 1.2 mM DPC. We studied M2FL in detergent micelles as opposed to lipid vesicles since light scattering would be less significant in comparison to lipid vesicles. Two different detergents were used, since the nature of the detergent could potentially affect the folding efficiency of the membrane protein[26,19]. Folding efficiency of the protein in the each detergent was compared by the ellipticity ratios at 223 and 209 nm ($\theta_{223}/\theta_{209}$) of its CD spectrum[24]. Increased intensity of molar ellipticity ratio of 223 to 209 nm would indicate a shift in the formation of tetramers.

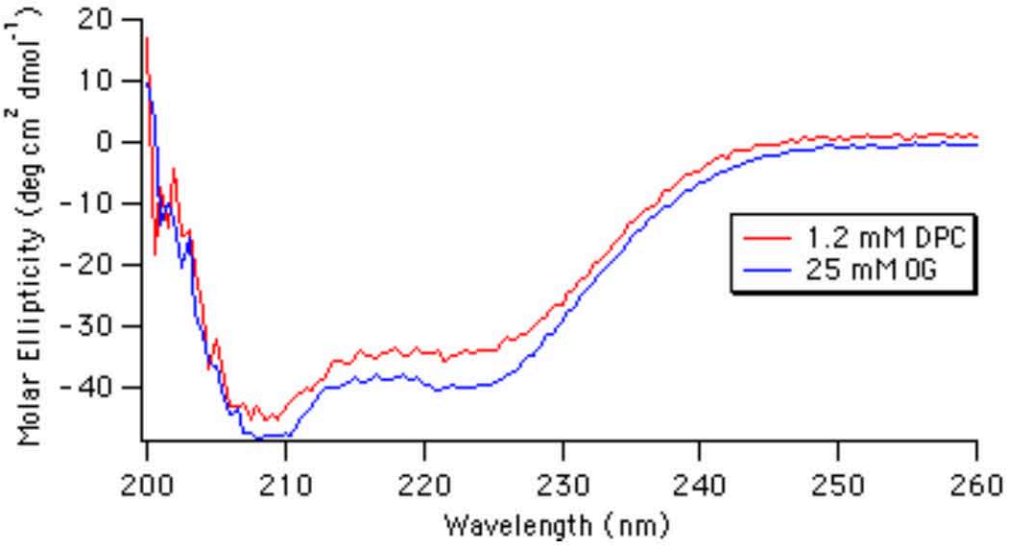

Figure 3.4. M2FL-WTe reconstituted in either 1.2 mM DPC micelles (red) or 25 mM OG micelles (blue).

Figure 3.4 indicated that at their respective CMCs, M2FL-WTe exhibited alpha helical character in OG compared to DPC. The ellipticity ratio for M2FL-WTe in OG was 0.84 compared to the ellipticity ratio of 0.77 for M2FL-WTe in DPC. Despite the increased alpha helical character, which suggested the improvement of folding of M2FL-WTe in OG, the high concentration of detergent required is undesirable due to associated

high degree of light scattering. Furthermore since difference in alpha helical character gained by the protein in OG micelles compared to DPC micelles is not large, it is desirable to utilize the less quantity demanding DPC detergent so to avoid unnecessary material expenses.

3.3. Interaction of M2FL-WTe with rimantadine in DPC micelles

Rimantadine and amantadine are drugs that inhibit influenza A replication by binding to the M2 channel, preventing the acidification of the virion after endocytosis. Both drugs have been shown to inhibit proton conductance by sterically blocking the proton channel[14]. The drug binding interaction has been shown to lead to notable increases in ellipticity ratio (223/209 nm) of the CD spectrum of the M2TM truncation of the M2 protein (Figure 3.5)[24,25]. Furthermore, rimantadine is known to stabilize the M2TM (res 22-46) tetramer to a greater extent than amantadine (Figure 3.5)[24, 25]. Given the notable changes in the CD spectra of M2TM by the titration of amantane inhibitors, the spectral changes in the CD by the titration of rimantdine to M2FL are investigated to compare to earlier M2TM results.

CD measurements were made using an Aviv 720 circular dichrometer at 25 °C. The CD spectra were recorded from six average stepwise scans from 260 to 198 nm with averaging time of 0.3333 seconds using a 1 mm quartz cell. Appropriate amount of M2FL-WTe dissolved in TFE was measured into a glass vial, and the sample was placed under gentle stream of N_2 to eliminate the organic solvent. The protein film was further freeze-dried under high vacuum for 12 hrs. After freeze-drying, the protein film was hydrated with buffer containing 50 mM Tris (pH 8.0), 100 mM KCl. In the final sample, the protein concentration was 50 μM and the DPC concentration was 5 mM. DPC

concentration of 5 mM was chosen to enable comparison to previous M2 CD results[25]. The ellipticity ratio (223/209) was calculated by averaging the ellipticity of 233 ±2 nm and 209 ± 2 nm to improve signal-to-noise[24].

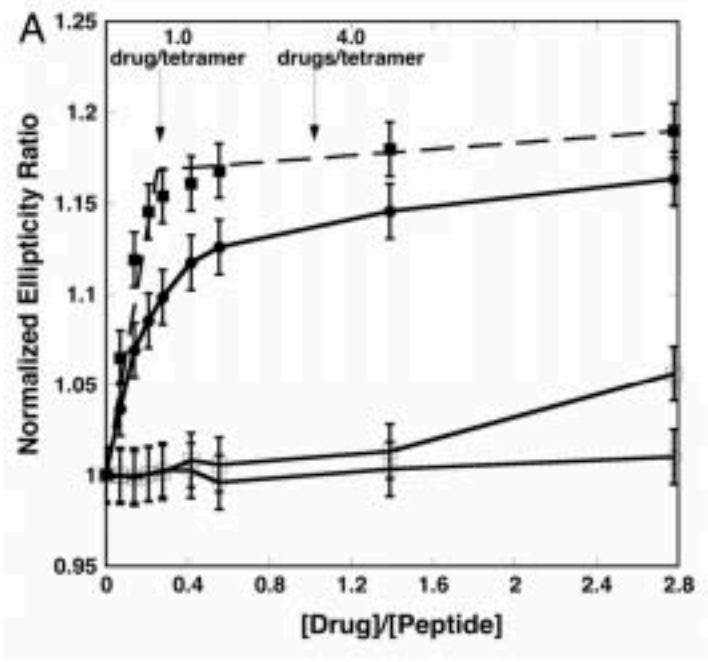

Figure 3.5. Normalized ellipticity ratio (223/209 nm) of as a function of [Drug]/[Peptide]. Titration of M2TM with rimantadine (square) compared to the titration of M2TM with amantadine (circle) showed that rimantadine leads to more significant stabilization compared to amantadine. Bottom two lines represent drug resistant M2TM constructs, which do not show increase in ellipticity ratio. Peptides were reconstituted in DPC micelles. Figure adapted from Ma, et. al, *PNAS*, (2000).

Titration of M2FL-WTe in DPC with rimantadine resulted in insignificant change in ellipticity ratio compared to M2TM. Also note that the ellipticity ratios of M2TM and M2TMC peptides binding to amantadine are between 0.95-1.10, which are much higher than what is observed for M2FL[25].

There are possible reasons for the lack of change in the ellipticity ratios in the titration of rimantadine to M2FL. It is possible that M2FL is misfolded in DPC such that the drug binding site is obscured. Another possibility is that the equilibrium constant from monomers to tetramers for M2FL-WTe is already largely

in favor of tetramer formation, as a consequence of additional stabilization brought about by its greater size so the change seen in M2TM is not observed. The latter possibilty seems more likely, but the CD data alone is insufficient in demonstrating the effect of titration of M2FL-WTe with rimantadine.

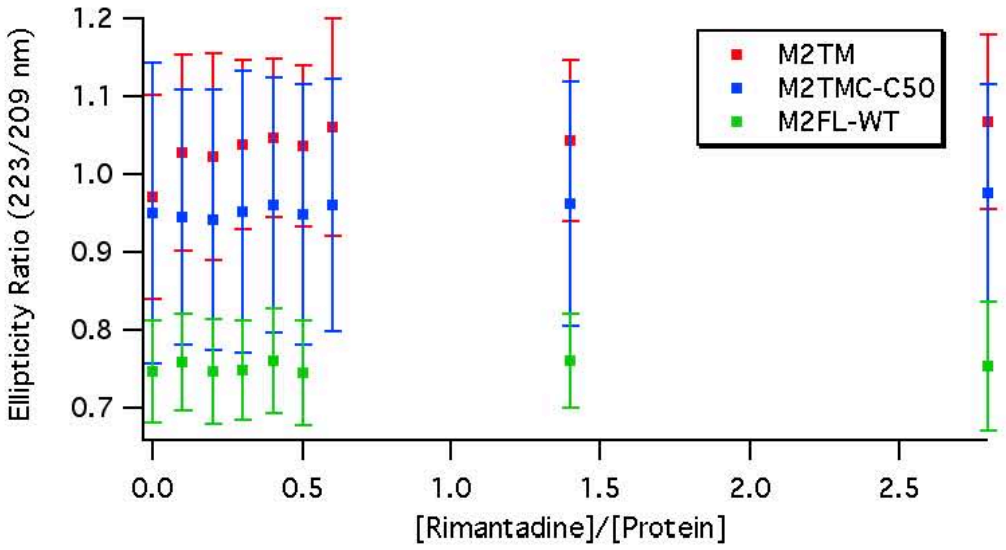

Figure 3.6. Ellipticity Ratio (223/209 nm) as a function of [Rimantadine]/[Protein]. Samples contained 50 μM protein, 5 mM DPC, 50 mM Tris (pH 8), 100 mM KCl.

Chapter 4: Spin-labeling Single-Cys Mutations of M2FL and EPR spectroscopy of M2FL-Cys in OG Micelles

4.1 SDSL EPR Spectroscopy

4.1.1 Background on Electron Paramagnetic Resonance Spectroscopy

Electron paramagnetic resonance (EPR) spectroscopy detects chemical species containing unpaired electrons. EPR measures the interactions between the magnetic field and unpaired electrons. In EPR spectroscopy, an external field causes an energy separation between two electron spin-states. Electromagnetic radiation in the form of microwaves is applied to the sample at a constant frequency, while the external magnetic field is increased. Resonance is observed when the energy of a photon is equal to the energy difference between two spin states (Figure 4.1).

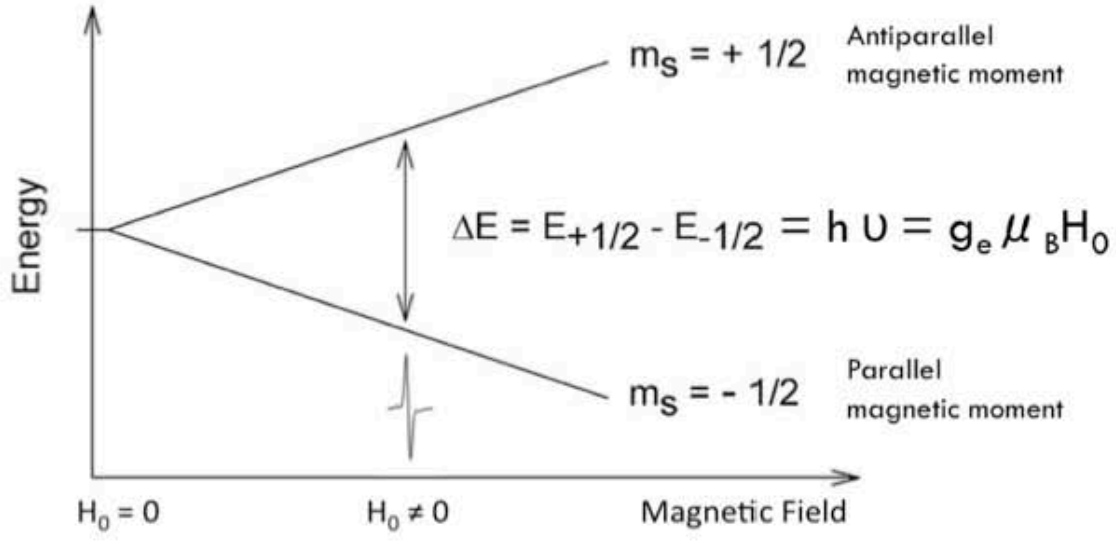

Figure 4.1. The resonance condition for EPR spectroscopy. An external magnetic field (H_0) causes separation in energy (ΔE) between two spin states of unpaired electrons. When the energy is equal to $\Delta E = g_e \mu_B H_0$, resonance is observed. Figure adapted from[27].

Electrons can occupy spin states of either +1/2 or -1/2, and these states are degenerate in the absence of an external magnetic field. Upon application of an external magnetic field, the magnetic dipole of the lone-pair electron can either align with or align against the magnetic field, leading to different energy states with an energy difference that is proportional to the magnetic field strength[27] (Figure 4.1). The energy difference, ΔE, is defined as

$$\Delta E = g\mu_B H_0$$

where g is defined as the spectroscopic splitting factor that is intrinsic to the sample, μ_B is the Bohr magneton and H_0 is the magnetic field strength[27]. The appearance of a mult-lined EPR spectrum depends on a number of parameters. The spacing between lines on the EPR spectrum is the result of hyperfine coupling, which is the interaction between an unpaired electron and nuclear spins. The number of peaks seen in a spectrum will be dependent on the spin state of the interacting nucleus if considering only hyperfine coupling. Thus, if **I** is the nuclear spin, then there will be 2**I**+1 peaks on the EPR spectrum. In case of the nitroxide spin lable, MTSL (see Section 4.1.2), the interaction between the lone pair electron with the 14N nucleus (**I** = 1), leads to three peaks in the EPR spectrum. No additional splitting is caused by nearby carbon and oxygen nuclei, as their most abundant isotopes have nuclear spins **I** = 0[27].

4.1.2 Site-directed spin labeling of proteins

Site-directed spin labeling (SDSL) allows EPR analysis of proteins. SDSL introduces a stable radical in the form of a spin-label to the protein, enabling the analysis of the environment as well as the dynamics of the location on the protein to which the spin-label is attached.

1-oxyl-2,2,5,5-tetramethyl-3-pyrroline-3-methyl methanethiosulfonate (MTSL; Toronto Research Chemicals, North York, Ontario, Canada) was chosen to label single-Cys mutants of M2FL. MTSL was selected because numerous examples in literature have demonstrated that single-site mutations to Cys and subsequent spin labeling with MTSSL lead to minimal perturbation of protein function in the majority of systems[28,29,30]. Minimal perturbation in function had been attributed to the small size of the EPR probe[27].

However, necessary controls for protein function should be conducted for each spin-labeled mutant, and sites that do lead to loss in function would not be analyzed. For example, Nguyen, et. al, spin labeled nine sites (residues 48-56) immediately C-terminal to the TM region of M2, and one spin-labeled construct showed perturbation in proton function[31]. The subject of an ongoing thesis in the Howard lab is developing a functional assay for membrane budding using expressed M2FL protein (Tae Kim '14). This method will be used to see if spin-labeled versions of M2FL lead to perturbations in function.

4.1.3. EPR Lineshapes Inform Protein Dynamics

EPR lineshapes also reflect the rotational motion of the nitroxide spin label in the range of 10^{-12} to 10^{-9} seconds[27]. When the motion of the spin label is fast (~0.1 ns) the EPR spectrum contains sharp peaks of equal height (Figure 4.2). When the motion of the spin label is restricted, the lines on the EPR spectrum broaden with decreasing overall amplitudes (Figure 4.2). In membrane proteins, the tumbling rate of the proteoliposomes is too slow to affect EPR lineshapes. Line broadening, therefore, reflects the motion of the spin label relative to the protein backbone[27]. Through-space dipole-dipole interactions with neighboring spin label less than 20 Å away also induces line

broadening, and broadening due to this effect is more prevalent in oligomers with multiple spin-labeled monomers[27].

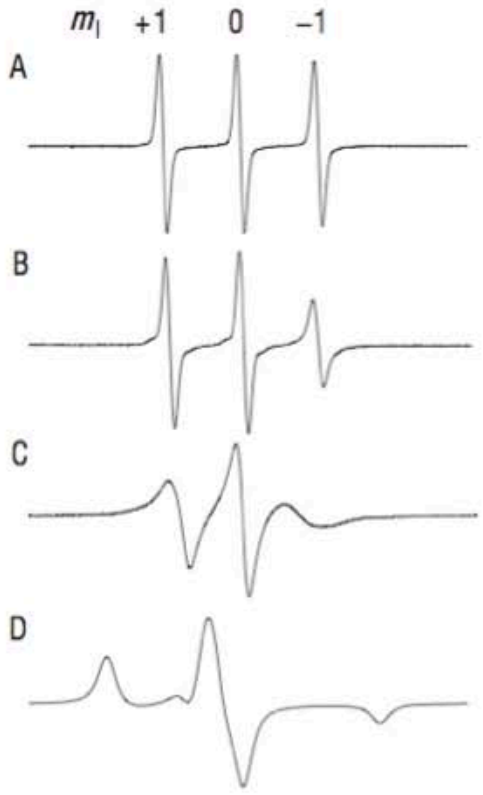

Figure 4.2. EPR spectra of MTSL under various degrees of motional restriction. (A) Dilute solution of MTSL showing fast rotation movement. (B) MTSL bound to 15-residue peptide in aq. solution. (C) Same peptide folded as an α-helix. (D) Spin-labeled peptide in frozen solution showing rigid limit spectrum.

4.2 Spin-labeling Reaction

The purification protocol was modified in order to facilitate the efficient spin-labeling of single-Cys mutants of M2FL. After washing the Ni-NTA resin with bound M2FL-Cys with Wash 3 buffer, the protein bound resin was then incubated overnight with 15 molar excess MTSSL spin-label, which was dissolved in labeling buffer

containing 50 mM Tris, 4 mM OG, and 20% v/v glycerol. Excess spin-labels were washed away using 20 column volumes of labeling buffer. After washing protein-bound resin of excess spin-label, the spin-labeled M2FL-Cys was eluted using 50 mM Tris (pH 8), 4 mM OG, 20% v/v glycerol, and 300 mM imidazole.

There are a number of reasons to spin-label M2FL-Cys during the last steps of its purification process. The SDS-PAGE gel of M2FL purification (Figure 2.3) demonstrates that Ni-NTA column purification is sufficient for purifying M2FL. Consequently, spin-labeling unknown species that are also annealed to the Ni-NTA matrix is minimal. Additionally, spin labeling of His-tagged monomeric species could minimize disulfide-bonded dimers in which Cys is not free to bind to the spin label. Lastly, excess spin-labels can be eliminated by eluting the Ni-NTA column with buffer, with retention of the spin-labeled protein.

4.2 Elimination of free-spin labels

4.2.1 Ni-Affinity Chromatography

Trace amounts of free spin-labels in solution leads to notably sharp signal that would interfere with the spectrum of the spin-labeled protein[27]. Therefore, it is important to remove free spin labels from the spin-labeled protein sample prior to SDSL EPR studies.

EPR spectra of eluant of the Ni-NTA column containing MTSL labeled M2FL-C19 had been collected in order to determine the minimum column volume required to fully eliminate free MTSL labels. Each column volume of eluant (~15 mL) was collected and stored separately. EPR spectra were taken at room temperature using an X-band Bruker EMX spectrometer with an ER4123D resonator. Samples were placed in glass

capillary tubes and EPR spectra were collected using 2 mW incident microwave power, 1 G field modulation amplitude at 100 kHz, and 150 G sweep width[31]. All spectra were acquired by averaging 100 scans in order to compare the intensities of signal resulting from free MTSL.

The EPR spectra of the eluant of the M2FL-C19-bound Ni-NTA column after labeling with MTSL revealed that free-spin labels could be fully eliminated through consecutive column washes with labeling buffer (Figure 4.1). EPR signal due to free MTSL was below the detection limit after 14 column volumes. Despite the effectiveness in eliminating free-spin labels associated repeated washes of the column with labeling buffer, efficiency of the process was largely lacking. Over 200 mL of wash buffer containing expensive detergent was required in order to obtain ~7.5 mg of spin-labeled M2FL. Consequently alternative purification protocols were investigated with aims to reduce the total volume of spin-labeling buffer required.

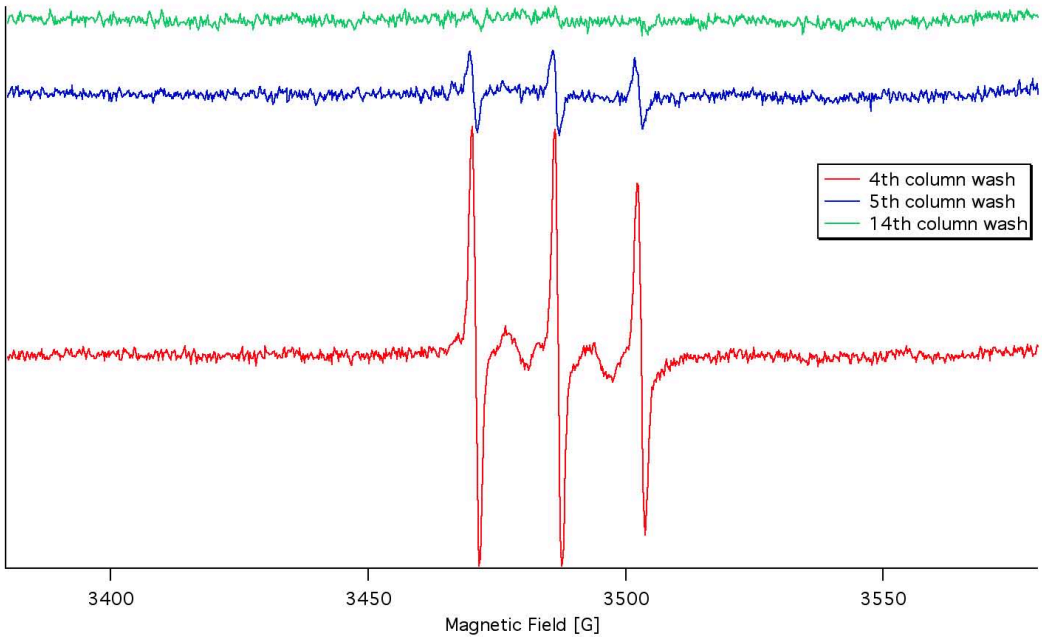

Figure 4.1. EPR spectra of column wash of MTSL labeled M2FL-C19 that had been annealed to Ni-NTA resin.

4.2.2 Size-Exclusion Chromatography coupled with Ni-Affinity Chromatography

Size-exclusion chromatography was investigated as a potential method for improving the efficiency of spin-labeling buffer usage. The large disparity between the molecular weights of the spin-labeled protein and free MTSL (12,172 Da/mol compared to 264.38 g/mol) suggested that separation between the spin-labeled protein and free MTSL would be sufficient. A PD-10 desalting column with exclusion limit of 5000 Da (GE Healthcare Life Sciences) was used to test out the effectiveness and efficiency of separation between spin-labeled M2FL and free MTSL. After eluting the MTSL-labeled M2FL-bound Ni-NTA column with ~50 mL of spin-labeling buffer, M2FL-C19 was eluted with 15 mL of elution buffer. M2FL-C19 was then concentrated to 2.5 mL using the Amicon Ultra-15 (Millipore) centrifuge concentrator and then loaded onto the PD-10 Desalting Column. After discarding the flow-through, spin-labeled M2FL-C19 was eluted using 3.5 mL of buffer. Eluted protein was fractionated in ~1 mL aliquots to determine the extent of separation between spin-labeled M2FL-C19 and free MTSL. Given the significant peaks corresponding to free MTSL (Figure 4.2), the protein sample was concentrated and eluted through a PD-10 Desalting Column for a total of three cycles.

Figure 4.2 showed the EPR spectra associated with each 1 mL fraction of the first cycle of purification by SEC. Presence of sharp peaks on all spectra suggested incomplete separation between M2FL-C19 and free MTSL. Dominance of free-spin character in the EPR spectrum of the 5th mL fraction (black) indicated that the fraction contained mostly free MTSL. Consequently, the 5th mL faction was discarded, and 5th mL fractions were of all subsequent SEC purifications were discarded as well. Not

included was the EPR spectrum of the 1st mL fraction, which showed no characteristic MTSL transitions.

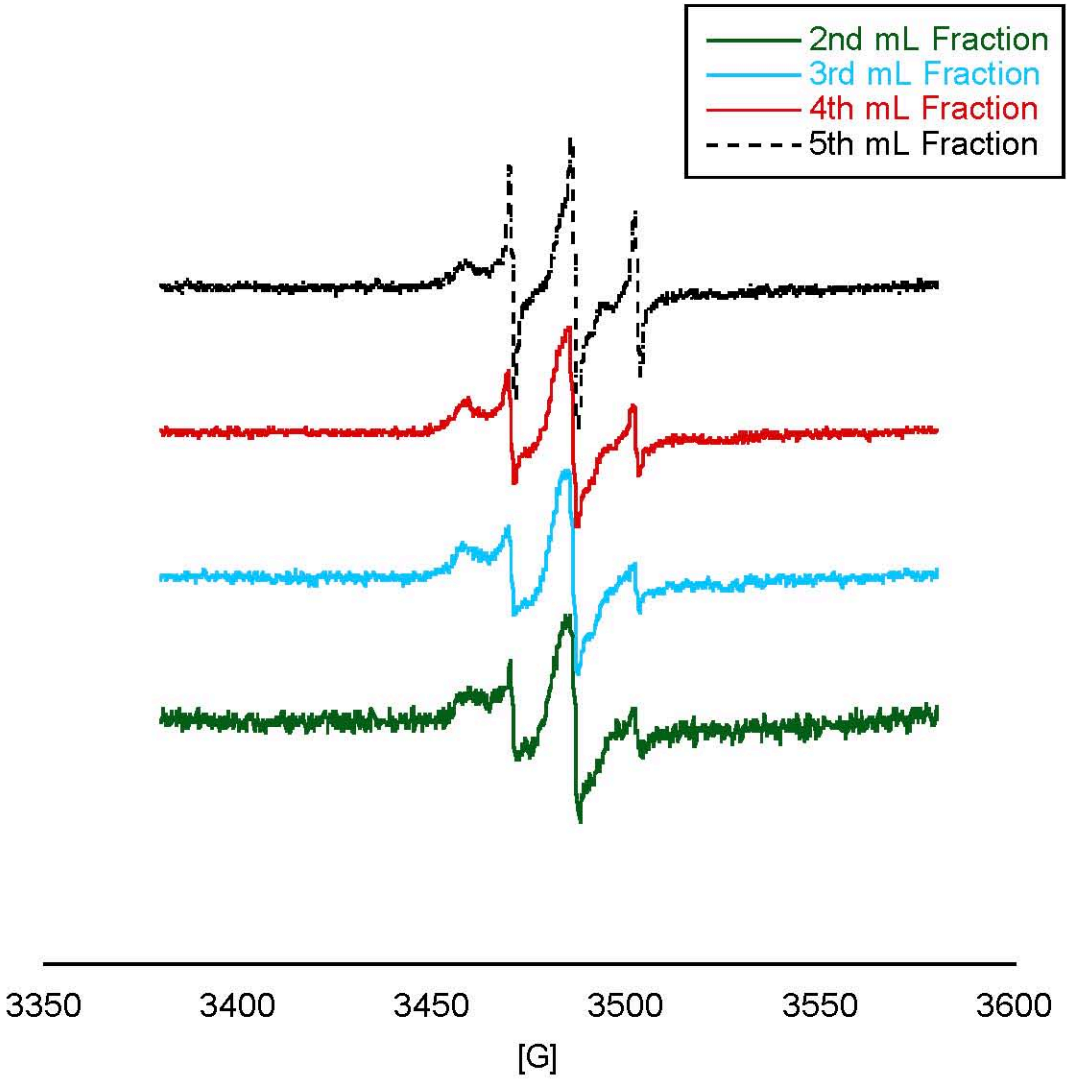

Figure 4.2. EPR spectra of ~1 mL fractions of eluted sample from the PD-10 Desalting column. This is the first of three purification cycles.

After the initial SEC purification, the collected spin-labeled M2FL-C19 fractions (factions 1-4) were recombined and concentrated for by SEC chromatography. Again, 1-mL fractions and the corresponding EPR spectra were collected (not shown). This

purification procedure was repeated for a third time. Figure 4.3 compared the EPR spectra of the 3rd mL fractions of each of the eluted samples of the three consecutive SEC purifications. The 3rd mL fraction was selected for comparison to look for improvement of separation because Figure 4.2 indicated that the 3rd mL fraction had both the highest concentration of spin-labeled M2FL-C19 as well as the least concentration of free MTSL. Comparing the three fractions, it was easy to spot the gradual elimination of free MTSL (from 1st cycle (green) to 2nd cycle (blue)), which corresponded to the decrease in intensity of sharp peaks (Figure 4.3). However, it is unclear as to why there is increased free MTSL from the second to third cycle of SEC purification (blue and red). One likely explanation could be that the SEC column was inadequately washed to remove free MTSL after the initial use. In the future, it would seem helpful to sample the wash of the SEC column to ensure the complete elution of the loaded sample prior to usage.

Following purification by SEC, the aliquots of spin-labeled M2FL-C19 were combined and its EPR spectrum was collected (Figure 4.4). Sharp signals present indicate that free MTSL is still detectable in the sample. However, the sharp signals that indicate the presence of free MTSL peaks can be eliminated by spectral subtraction of the EPR spectrum of a dilute solution of free MTSL with estimated concentration that is similar to that found in the spin-labeled protein sample.

Line broadening shown in the EPR spectrum of spin-labeled M2FL-C19 (Figure 4.4) with respect to the EPR spectrum of dilute MTSL (Figure 4.1) suggests that MTSL is attached to M2FL-C19. The motion of the spin-label is reduced because of its attachment to a much slower-moving protein, and the reduction in motion leads to line broadening, which is observed. Figure 4.4 also indicates that M2FL-C19 in 4 mM OG buffer possesses a significant broadened component as indicated by the arrow. There are multiple possible explanations for the presence of the broadened component. One possibility is that Cys-19 is deeply buried within the folds of the full-length protein, which restricts the mobility of the spin-label. Another possibility is that there is a high degree of packing of monomers within the OG micelles, leading to significant broadening due to through-space dipole-dipole interactions between spin-labels <20 Å apart.

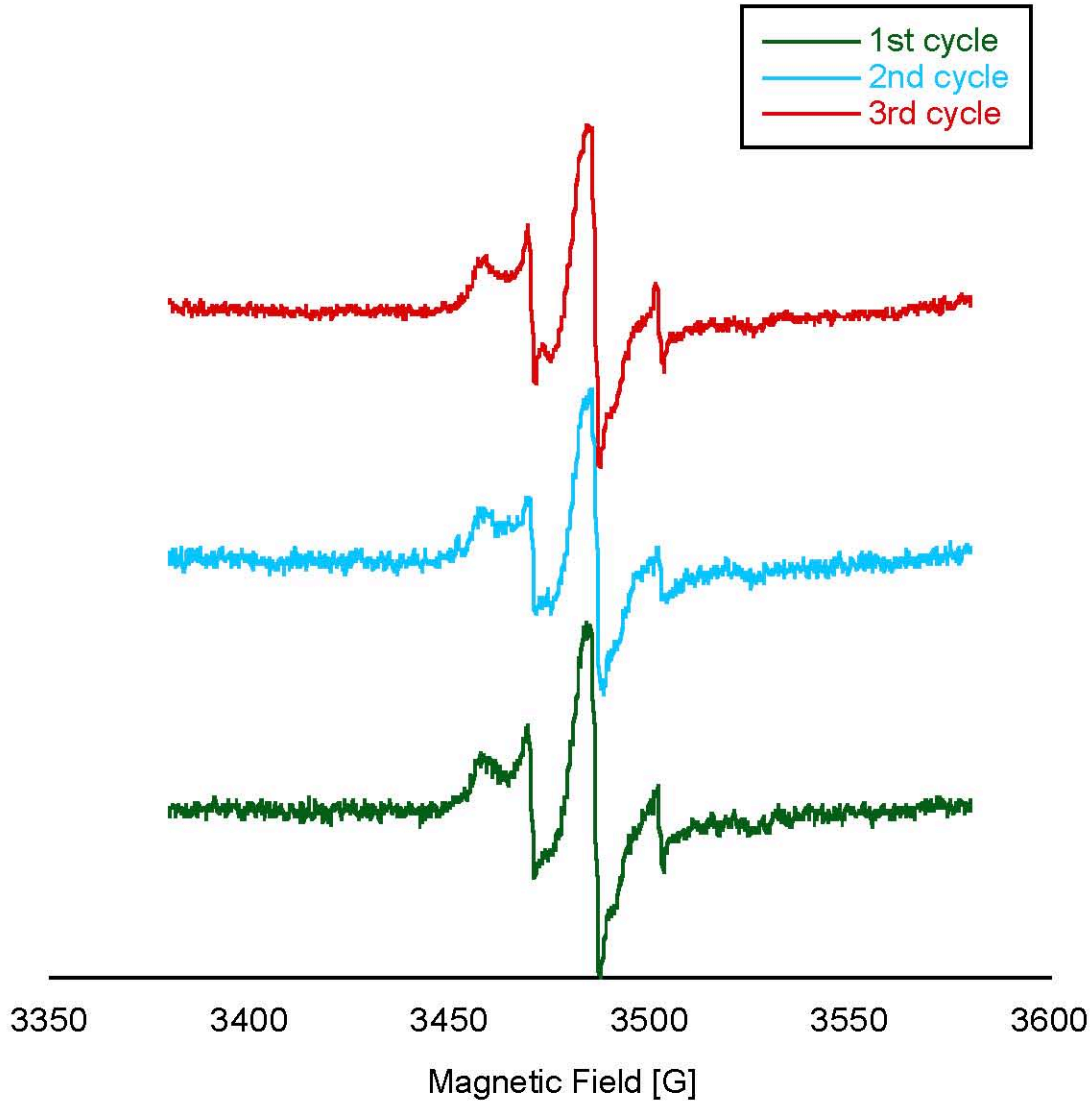

Figure 4.3. EPR spectra of the 3rd mL fraction of eluted samples corresponding to each of the three cycles of SEC purification.

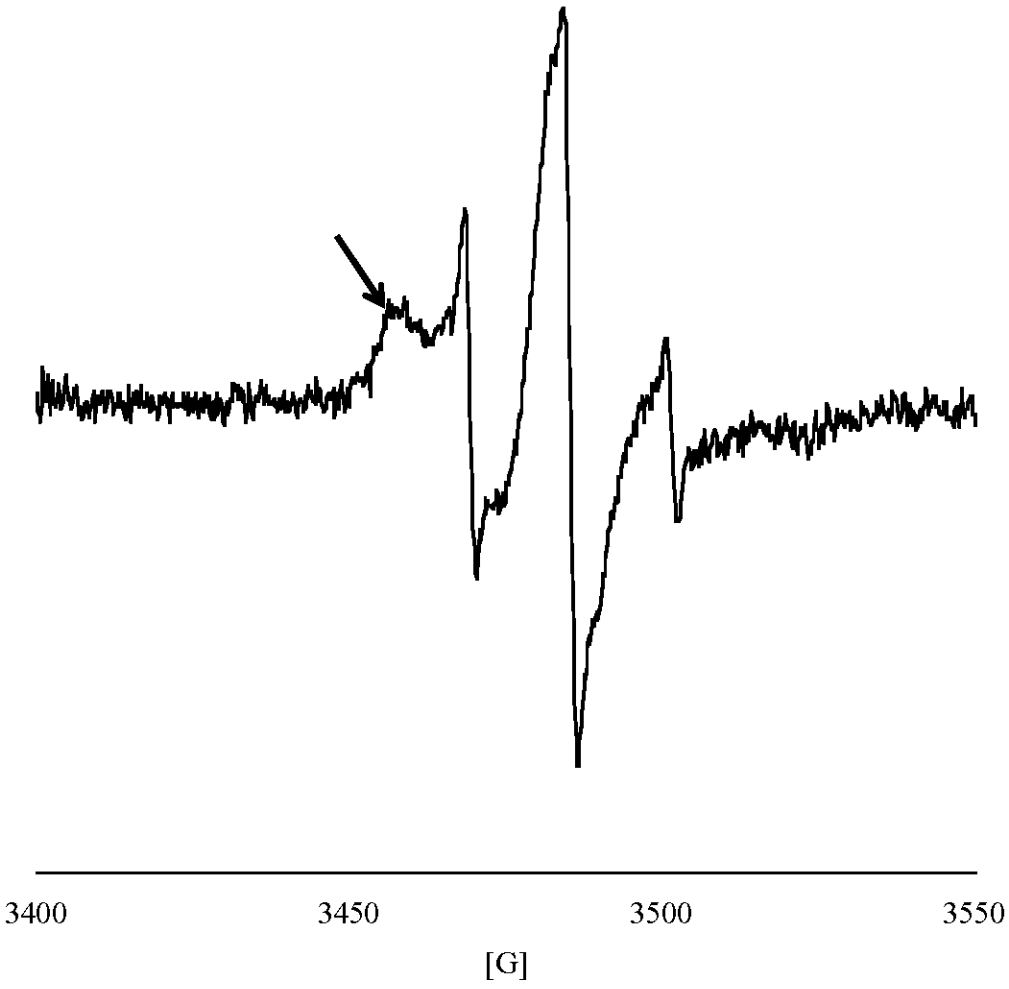

Figure 4.4. EPR spectrum of M2FL-C19 in buffer containing 50 mM Tris (pH 7.8), 4 mM OG, 20% v/v glycerol.

4.3 EPR spectrum of M2FL-C19 in OG buffer

To investigate the nature of the broadened component, EPR spectra of samples of M2FL-C19 solvated in varying concentrations of OG was collected. Buffer containing 50 mM Tris (pH 7.8), 20% v/v glycerol and varying concentrations of OG was added to a concentrated solution of M2FL-C19 in 4 mM of OG buffer to achieve desired concentration of detergent. Final concentration of spin-labeled protein achieved in all samples was 100 μM.

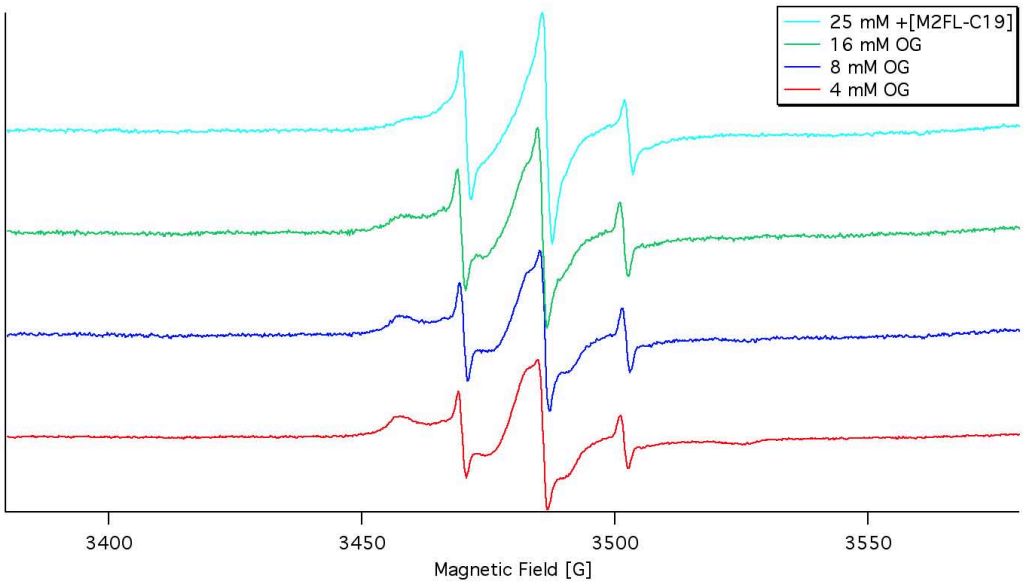

Figure 4.5. EPR spectrum of M2FL-C19 in varying concentrations of OG buffer with the addition of 50 mM Tris (pH 7.8), 20% v/v glycerol.

The broadened component observed in Figure 4.4 is due to high degree of packing amongst monomers of M2FL-C19. In can be observed that the intensity of the broad component decreases with increasing concentrations of OG detergent (Figure 4.5). This suggests that the distance between neighboring increases spin-labels with increasing concentrations of detergent micelles, leading to reduced through-space dipole-dipole interactions between neighboring spin-labels.

Chapter 5: Reconstitution of M2FL-C19 in Mixed Lipid Bilayers

5.1 Strategies for Reconstitution of M2 Truncations into Lipid Bilayers

Multiple strategies have been employed in literature for reconstituting synthetic truncations of M2 into lipid bilayers. One methodology employs recurring sonication and freeze-thaw cycles of the proteolipid mixture[32]. This method has been effective for both M2TM and M2TMC truncations[31]. Another method involves the addition of detergent as well as micelle solubilized M2 to previously generated lipid vesicles[13,14]. The addition of detergent destabilizes the preformed lipid vesicles, enabling the insertion of the membrane protein. To complete the reconstitution, detergent is gradually removed by dialysis[14] or the usage of hydrophobic polystyrene beads (Bio-Beads SM-2, Bio-Rad)[13]. While both methods appear effective reconstituting of M2 truncations into lipid bilayers, the latter method better complements the established protein purification methodology associated with M2FL and will be used.

5.2 Choice in Lipid Vesicle Composition

The model membrane system composed of a 4:1:1 molar ratio POPC:POPG:cholesterol lipid bilayer was selected for the reconstitution of M2FL. POPC (1-palmitoyl-2-oleoylphosphatidylcholine) (Avanti Polar Lipids) was chosen because its hydrophobic chain length is similar to those found in viral membranes[33]. Furthermore, POPC minimized the helical tilt of M2, which reduced unfavorable interactions between hydrophilic residues and the hydrophobic membrane[33]. POPG (1-palmitoyl-2-oleoyl-sn-glycero-3-phospho-(1'-rac-glycerol)) (Avanti Polar Lipids) possesses the same hydrophobic tails as POPC, and its charged head group was found to minimize lipid aggregation and optimize reconstitution of M2TMC into bilayers[31].

Cholesterol was added in the procedure to provide the option for future studies in the structural studies involving the interaction between full-length M2 and cholesterol in facilitating viral budding[10].

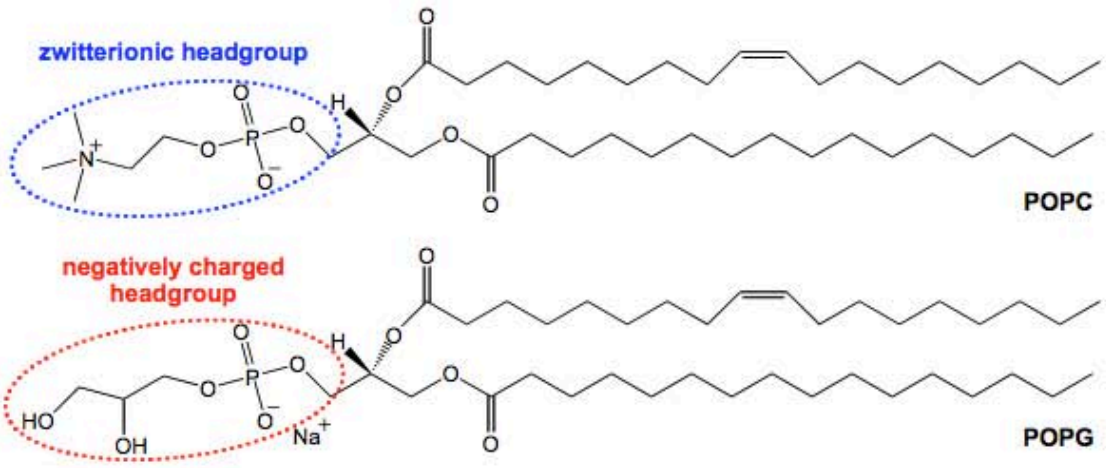

Figure 5.1. Structure of POPC and POPG lipids used in creating the 4:1:1 POPC:POPG:cholesterol lipid vesicles for reconstituting M2FL. Figure adapted from[31].

5.3 Methods Used for Reconstitution of M2FL into Mixed Lipid Bilayers

Molar composition of 4:1:1 POPC:POPG:cholesterol was produced by mixing lipids which had been stored in chloroform. Solvent was evaporated under a gentle stream of nitrogen followed by further drying high vacuum for 12 hrs. Lipids were then resuspended in aqueous buffer consisting of 50 mM Tris (pH 7.8) and 100 mM KCl, vortexed and sonicated until evenly mixed. The lipid mixture was then extruded 15 times through a 200 nm polycarbonate filter. The formed vesicles were then solubilized with OG to a molar detergent-to-lipid ratio of 2.6 (CMC was subtracted from the total detergent concentration). M2 was then added to a molar ratio of lipid to protein of 500. 20 mg of hydrophobic polystyrene beads (Bio-Beads SM-2, Bio-Rad) per milligram of OG were subsequently added, and the resulting suspension was placed on a gently rocking platform for 3 hrs at 4 °C to remove OG and facilitate the formation of M2

proteoliposomes. M2 proteoliposomes were carefully extracted from the slurry following brief centrifugation.

5.4 Success of M2FL Reconstitution into Lipid Bilayer Indicated by EPR

The EPR spectrum of M2FL-C19 reconstituted in 4:1:1 POPC:POPG:cholesterol vesicles exhibits line broadening with respect to that of M2FL-C19 solubilized in 4 mM OG detergent (Figure 5.2). M2 is marginally more stabilized and samples fewer random conformational states in the described model membrane system compared to OG micelles. Comparing the structure of OG (Figure 3.2) against that of POPC and POPG (Figure 5.1) shows that OG possesses significantly shorter hydrophobic chain length, which is destabilizing and leads to larger numbers of random conformations than POPC:POPG:cholesterol lipid vesicles. Thus, the observed broadening in the EPR spectrum of M2FL-C19 in 4:1:1 POPC:POPG:cholesterol vesicles relative to that of M2FL-C19 solubilized in 4 mM OG detergent show that M2 is marginally stabilized by the lipid vesicles and more motionally restricted, indicating the success of protein reconstitution.

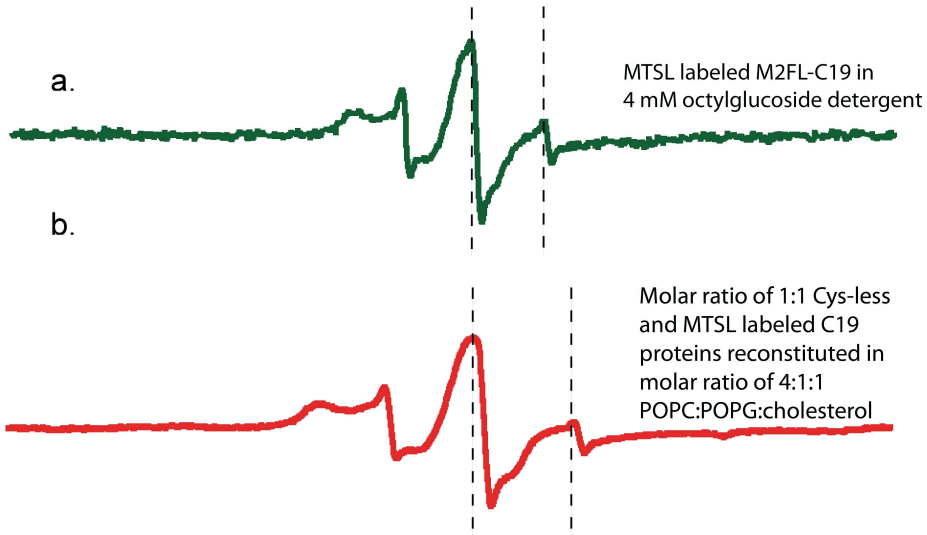

Figure 5.2. EPR spectra of (a) MTSL labeled M2FL-C19 in 4 mM octylglucoside detergent buffer and (b) 1:1 molar ratio of MTSL labeled C19 and unlabeled M2FL reconstituted in molar ratio of 4:1:1 POPC/POPG/cholesterol vesicles.

Chapter 6: Conclusions and Future Directions

6.1 Conclusions

Methods for the overexpression and purification have been developed for the full-length M2 protein (Appendices B and C). Furthermore, the full-length M2 protein has been characterized in detergent micelles using CD and EPR spectroscopy. Successful methods for spin-labeling and reconstitution of M2FL-C19 in lipid vesicles consisting of molar ratio of 4:1:1 POPC:POPG:cholesterol had been developed and preliminary studies have been carried out.

6.2 Future Directions

The Howard lab currently has in possession transformed *E. Coli* cells for 10 single-site Cys mutants of M2FL. Single Cys placed at positions 50-60 in M2FL will allow us to scan the amphipathic C-terminal helix we have already studied in the M2TMC truncation by EPR[31]. Furthermore, this region is of particular interest recently due to its suspected role in viral budding[10].

A functional assay for membrane budding will also be developed for the full-length M2 (Tae Kim '14) to provide proper controls to ascertain the functional relevancy of the single-site Cys mutants of M2FL.

Acknowledgements

I would like to thank Dr. Kathleen Howard for her constant support and guidance throughout this research. I would also like to thank Jessica Thomaston, Dr. Jun Wang, and Dr. Bill DeGrado at University of California San Francisco for providing the transformed *E. Coli* cells for the full-length M2 mutants. I am extremely grateful for the financial support provided by the Howard Hughes Medical Institute of Swarthmore College. I would also like to thank members of the Howard lab, Tae Kim ('14), Shawn Kim ('14), and Matt Elkins ('14) for their companionship and support throughout my time in the Howard lab.

Appendix A: Nucleotide sequence of M2FL-C50 plasmid S50CP1

Note: T7 reverse primer was used, so sequence shown here would be the reverse complement of the actual results)

Nucleotide sequence:
>KM_311096-502_S50CP1_T7-Reverse_F08_reverse-complement
NNGNNNTNNNTTNNTCCNNNNNNNNNNCNNNNNCNNNCNNTNNNNNNNNGNN
NNNNNNNNNNNNNCNNNNNTNNCNNNNNNNNNNNGNNGNTNNGNNNNNNC
NTNAGNGNNNTNGNNANNGNTNACANNNNNNNNCNNNTCNNNNNNNCAGNN
NNTNANNNNTCCAGAAGCNTAANNTNNNGNTNTGATAAAGNNNNCANNNTA
NGGGCGGTTTTTNNNNNTNNGTCACTGATGCCTCCGTNNTAAGGGGGATTT
CTGTTCATGGGGGTAANGATACCGATGAAACGAGAGAGGATGCTCACGATAC
GGGTTACTGATGATGAACATGCCCGGTTACTGGAACGTTGTGAGGGTAAACA
ACTGGCGGTATGGATGCGGCGGGACCAGAGAAAAATCACTCAGGGTCAATG
CCAGCGCTTCGTTAATACAGATGTAGGTGTTCCACAGGGTAGCCAGCAGCAT
CCTGCGATGCAGATCCGGAACATAATGGTGCAGGGCGCTGACTTCCGCGTTT
CCAGACTTTACGAAACACGGAAACCGAAGACCATTCATGTTGTTGCTCAGGT
CGCAGACGTTTTGCAGCAGCAGTCGCTTCACGTTCGCTCGCGTATCGGTGATT
CATTCTGCTAACCAGTAAGGCAACCCCGCCAGCCTAGCCGGGTCCTCAACGA
CAGGAGCACGATCATGCGCACCCGTGGCCAGGACCCAACGCTGCCCGAGATC
TCGATCCCGCGAAATTAATACGACTCACTATAGGGAGACCACAACGGTTTCC
CTCTAGAAATAATTTTGTTTAAGAATTCGAAGGAGATATACCATGAGCCTGCT
GACCGAAGTGGAAACCCCGATTAGAAATGAATTTGGCAGCCGCAGCAACGAT
TCATCGGATCCTCTGGTTGTTGCGGCGAGCATCATTGGCATCTTGCACTTGAT
TTTGTGGATTCTGGATCGTCTGTTTTTCAAATGCATCTATCGATTCTTTGAACA
TGGTCTGAAACGCGGCCCGTCTACCGAAGGCGTGCCGGAATCTATGCGCGAA
GAATATCGCAAAGAACAGCAGAGCGCGGTGGATGCCGATGATAGTCATTTTG
TGAGCATTGAAGGCCGCCACCACCACCACCACCACTAAGCATGCAAAAAAA
AAAAAAAAAAAGCTTGCGGCCGCACTCGAGCACCACCACCACCACCACTGA
GATCCGGCTGCTAACAAAGNNCGAANNNANNNNNNN

ExPASy translation to amino acids:
5'3' Frame 1
X X X X X X X X X X X X X X X X X X X X X X X X X X X X X X X X X X X X X
X X X X T X X X X X X X X X X X X X Q K X X X X X X **Stop** **Stop** X X X X X G G F X
X X X H **Stop** C L R X K G D F C S W G **Stop** X Y R **Stop** N E R G C S R Y G L L
Met **Met** N **Met** P G Y W N V V R V N N W R Y G C G G T R E K S L R V N A S A S
L I Q **Met** **Stop** V F H R V A S S I L R C R S G T **Stop** W C R A L T S A F P D F T K
H G N R R P F **Met** L L L R S Q T F C S S S R F T F A R V S V I H S A N Q **Stop** G N
P A S L A G S S T T G A R S C A P V A R T Q R C P R S R S R E I N T T H Y R E T
T T V S L **Stop** K **Stop** F C L R I R R R Y T **Met** S L L T E V E T P I R N E F G S R S
N D S S D P L V V A A S I I G I L H L I L W I L D R L F F K C I Y R F F E H G L K
R G P S T E G V P E S **Met** R E E Y R K E Q Q S A V D A D D S H F V S I E G R H H
H H H H **Stop** A C K K K K K K A C G R T R A P P P P P L R S G C **Stop** Q X X X X
X X X

Appendix B: Optimized protocol for Overexpression for M2FL

Protein Expression in LB medium

1. Prepare LB/agar for plates and LB media for expression and autoclave. See Instructions for preparation of LB/agar plates in the "General Molecular Biology" section of the Howard Lab Protocol Binder. Two 1 L growths typically done at once. Don't forget to make extra batches of LB for starting cultures and dilution of cell pellets. Two extra 100 mls batches made in special 100 ml bottles should be enough. Also autoclave a 100 ml flask for overnight culture.

1. Prepare a LB agar plate with 100 μg/ml ampicillin. See Instructions for preparation of LB/agar plates in the "General Molecular Biology" section of the Howard Lab Protocol Binder. Note plates take ~24 hours to dry before they can be streaked with cells.

2. Remove glyercol stock from -80 freezer and place it in a bucket filled with ice. Streak plate with glycerol cell stock. See Instructions for use of sterile techniques in the "General Molecular Biology" section of the Howard Lab Protocol Binder. Plate incubated at 37°C overnight in shaker without shaking.

3. A single colony was picked up from the plate to inoculate 5ml LB in sterile falcon tube supplemented with 100 μg/ml ampicilin, and was allowed to incubate at 37 °C with 160 rpm shaking for 8 hrs.

4. Next, 0.5 ml of the above cell solution was used to inoculate 50 ml of LB supplemented with 100 μg/ml ampicilin and shake at 37 °C overnight.

5. The overnight culture was used to inoculate 1 L of LB supplemented with 100 μg/ml ampicillin and allowed to incubate at 37 °C with 160 rpm shaking.

6. ODs checked using HP Diode Array spectrophotometer in Biochemistry Resource Room using plastic cuvettes. See directions for OD measurements in General Molecular Biology" section of the Howard Lab Protocol Binder.

7. When OD600 reached 0.7–1.0 (normally after 2 hrs), M2 expression was induced with 1 mM IPTG. Stocks of IPTG kept in freezer.

8. After IPTG induction ODs were checked at 2 hr and 3 hrs. Protein expression was halted at ~3 hrs by centrifugation using Legend R++ benchtop centrifuge in Biochem Resource Room. Centrifuge turns on with switch on the right side of instrument. Drop temperature to 4°C. Split growth media into four 750 ml centrifuge tubes. Balance them using top loader balance. Settings: 9 acc/5 dec/spin at 4000 rpm for 30 minutes.

9. Pour off most of supernatant, which can then be discarded. Use fresh LB to resuspend pellets and transfer them to 50 ml falcon tubes. Balance, and re-spin using same centrifuge setting as the previous step.

10. Pour off supernatant and discard. Invert tubes on paper towels to dry off pellets. Cell pellets can be stored in cardboard box in -80 freezer until you are ready for purification.

Appendix C: Optimized Purification and Spin-labeling Protocol for M2FL

References:

1. Leiding, et. al. (2010). PNAS. 107(35) 15409.
2. The QIAexpressionist (2003).
3. Klugg. (7/02/12). E-mail.

Abbreviations:

OG: n-octyl-β-D-glucoside
AEBSF hydrochloride: 4-(2-Aminoethyl) benzenesulfonyl fluoride hydrochloride (protease inhibitor)
MTSSL: 1-oxyl-2,2,5,5-tetramethyl-3-pyrroline-3-methyl methanethiosulfonate
ACN: acetylnitrile

Stock solutions:

Standard buffer (50 mM Tris (pH 8), 150 mM NaCl, 40 mM OG): Mix 5 mL 1 M Tris pH 8.0, 0.88 g NaCl, 1.17 g OG, and 95 mL Millipore water. Store at 4 °C.

10 mg/mL DNase I: 10 mg DNase I in 1 mL of standard buffer. Store at -20 °C. Stock solution is stable for up to 4 freeze-thaws.

100 mM AEBSF: 50 mg AEBSF Hydrochloride in 2.09 mL standard buffer. Store at -20 °C. Stock solution is stable for up to 1 month.

10 mg/mL lysozyme stock: 10 mg of lysozyme in 1 mL of standard buffer. Store at -20 °C. Stock solution is stable for up to 4 freeze-thaws.

Lysis buffer (50 mM Tris(pH 8), 40 mM OG, 150 mM NaCl, 0.02 μg/mL DNase I, 500 μM AEBSF and 0.25 μg/mL lysozyme): Mix 100 mL of standard buffer, 2 μL DNase I stock, 500 μL of AEBSF stock, and 2.5 μL of lysozyme stock.

Wash I (50 mM Tris (pH 8), 150 mM NaCl, 40 mM OG, and 20% v/v glycerol): 5 mL 1M Tris (pH 8), 0.88 g NaCl, 1.17g OG, 20 mL glycerol, and 80 mL Millipore water.

Wash II (50 mM Tris (pH 8), 20 mM OG, 20% v/v glycerol): 5 mL 1 M Tris (pH 8), 0.59 g OG, 20 mL glycerol, 80 mL Millipore water.

Wash III (50 mM Tris (pH 8), 4 mM OG, 20% v/v glycerol, 20 mM imidazole): 5 mL 1 M Tris (pH 8), 0.12 g OG, 20 mL glycerol, 0.137 g imidazole, and 80 mL Millipore water.

Elution buffer (50 mM Tris (pH 8), 4 mM OG, 20 % v/v glycerol, 300 mM imidazole): 5 mL 1 M Tris (pH 8), 0.12 g OG, 20 mL glycerol, 2.04 g imidazole, and 80 mL Millipore water.

Column labeling buffer: (50 mM Tris (pH 8), 4 mM OG, 20 % v/v glycerol: 5 mL 1 M Tris (pH 8), 0.12 g OG, 20 mL glycerol

MTSSL stock solution (200 mM): Dissolve 5.3 mg of MTSSL spin-labels in 100 μL of ACN.

Protein purification (Expected yield for M2FL-C19 is 15 mg/L of E. Coli growth):

1. Resuspend cell pellet in lysis buffer. Use ~50 mL of lysis buffer per liter of growth. Pool into one Falcon tube.
2. Sonicate cell pellet suspension on ice water suspension using the bath sonicator. Lyse cells by carrying out 30 cycles of 15 sec sonication and 10 end-over-end inversions with 20 sec vortexing after every 10 cycles of sonication and end-over-end inversions.
3. Centrifuge lysis solution at 16,000 rpm at 4 °C with F185-12X50 rotor in floor centrifuge in Biochem Resource Room for 30 min. Save supernatant for Ni-NTA column purification. (Obtain 10 µL of lysate for SDS-PAGE gel electrophoresis).
4. While lysis solution is being centrifuged, pour 1.5 mL of resin into 1 mL plastic column. Elute the 10% EtOH that the resins are stored in and equilibrate with 2 column volumes of Millipore water followed by 2 column volumes of standard buffer. (Use ~ 1 mL of resin for 5-10 mg of expected protein).
5. Incubate 25 mL of supernatant in 1.5 mL of Ni-NTA super flow resin (Qiagen) and 20 mM imidazole in cold room for 30 min with gentle shaking using a nutator. (Expected protein yield for M2FL-C19 is 7.5 mg/mL)
6. Wash columns successively with Wash I, Wash II, and Wash III solutions. Use 10 column volumes each to ensure that all impurities are removed.
7. Add 15x molar MTSSL to 3 mL Wash II solution. (47 µL of MTSSL stock solution)
8. Cap bottom of column and add buffer with spin label to column. Let buffer flow onto resin. Cap top of column and wrap column with aluminum foil. Let the columns incubate/shake on nutator overnight in cold room (4 °C)
9. Uncap column and let buffer run through.
10. Wash away excess free spin-labels using 20 column volumes of column labeling buffer solution.
11. Elute protein using 10 column volumes of elution buffer.
12. Concentrate the protein using the Amicon Ultra-15 by centrifuging at 3,500g for 10 mins and homogenizing protein solution using a pipetter.
13. Repeat step 14 until reaching a desired protein concentration (~5.5 mM; check protein concentration by nanodrop)
14. Check the eluant in the Amicon Ultra-15 for absorbance at 280 nm to confirm the absence of protein.

Works Cited

1. Ganatra, R.; Kniss, K.; Epperson, S.; Blanton, L.; Mustaquim, D.; Bishop, A.; D'Mello, T.; Perez, A.; Dhara, R.; Brammer, L.; Chaves, S.; Gubareva, L.; Wallis, T.; Xu, X.; Bresee, J.; Klimov, A.; Cox, N.; Finelli, L.; S, W. H. O. C. C., Update: Influenza Activity-United States, 2011-12 Season and Composition of the 2012-13 Influenza Vaccine (Reprinted from MMWR, vol 61, pg 414-420, 2012). *Jama-Journal of the American Medical Association* **2012,** *308* (9), 854-858.
2. Maugh, T., Swine flu danger appears to be ebbing. Los Angeles Times: 2010.
3. Rossman, J.; Lamb, R., Influenza virus assembly and budding. *Virology* **2011,** *411* (2), 229-236.
4. Roberts, P.; Compans, R., Host cell dependence of viral morphology. *Proceedings of the National Academy of Sciences of the United States of America* **1998,** *95* (10), 5746-5751.
5. Goto, H.; Kawaoka, Y., A novel mechanism for the acquisition of virulence by a human influenza A virus. *Proceedings of the National Academy of Sciences of the United States of America* **1998,** *95* (17), 10224-10228.
6. Graphical Representations of a Generic Influenza Virus. 2009.
7. Pinto, L.; Lamb, R., Controlling influenza virus replication by inhibiting its proton channel. *Molecular Biosystems* **2007,** *3* (1), 18-23.
8. Wang, J.; Qiu, J.; Soto, C.; DeGrado, W., Structural and dynamic mechanisms for the function and inhibition of the M2 proton channel from influenza A virus. *Current Opinion in Structural Biology* **2011,** *21* (1), 68-80.
9. Sugrue, R.; Bahadur, G.; Zambon, M.; Hallsmith, M.; Douglas, A.; Hay, A., Specific Structural Alteration of the Influenza A Hemaglutinin by Amantadine. *Embo Journal* **1990,** *9* (11), 3469-3476.
10. Rossman, J.; Jing, X.; Leser, G.; Lamb, R., Influenza Virus M2 Protein Mediates ESCRT-Independent Membrane Scission. *Cell* **2010,** *142* (6), 902-913.
11. Fiorin, G.; Carnevale, V.; DeGrado, W., The Flu's Proton Escort. *Science* **2010,** *330* (6003), 456-458.
12. Kochendoerfer, G.; Salom, D.; Lear, J.; Wilk-Orescan, R.; Kent, S.; DeGrado, W., Total chemical synthesis of the integral membrane protein influenza A virus M2: Role of its C-terminal domain in tetramer assembly. *Biochemistry* **1999,** *38* (37), 11905-11913.
13. Leiding, T.; Wang, J.; Martinsson, J.; DeGrado, W.; Arskold, S., Proton and cation transport activity of the M2 proton channel from influenza A virus. *Proceedings of the National Academy of Sciences of the United States of America* **2010,** *107* (35), 15409-15414.
14. Cady, S.; Wang, T.; Hong, M., Membrane-Dependent Effects of a Cytoplasmic Helix on the Structure and Drug Binding of the Influenza Virus M2 Protein. *Journal of the American Chemical Society* **2011,** *133* (30), 11572-11579.
15. Wang, J.; Ma, C.; Fiorin, G.; Carnevale, V.; Wang, T.; Hu, F.; Lamb, R. A.; Pinto, L. H.; Hong, M.; Klein, M. L.; DeGrado, W. F., Molecular dynamics simulation directed rational design of inhibitors targeting drug-resistant mutants of influenza A virus M2. *J Am Chem Soc* **2011,** *133* (32), 12834-41.
16. Grandea, A.; Olsen, O.; Cox, T.; Renshaw, M.; Hammond, P.; Chan-Hui, P.; Mitcham, J.; Cieplak, W.; Stewart, S.; Grantham, M.; Pekosz, A.; Kiso, M.; Shinya, K.;

Hatta, M.; Kawaoka, Y.; Moyle, M., Human antibodies reveal a protective epitope that is highly conserved among human and nonhuman influenza A viruses. *Proceedings of the National Academy of Sciences of the United States of America* **2010,** *107* (28), 12658-12663.
17. Dawson, P.; Kent, S., Synthesis of native proteins by chemical ligation. *Annual Review of Biochemistry* **2000,** *69*, 923-960.
18. Schnell, J.; Chou, J., Structure and mechanism of the M2 proton channel of influenza A virus. *Nature* **2008,** *451* (7178), 591-U12.
19. Cross, T.; Sharma, M.; Yi, M.; Zhou, H., Influence of solubilizing environments on membrane protein structures. *Trends in Biochemical Sciences* **2011,** *36* (2), 117-125.
20. Takeuchi, H.; Okada, A.; Miura, T., Roles of the histidine and tryptophan side chains in the M2 proton channel from influenza A virus. *Febs Letters* **2003,** *552* (1), 35-38.
21. Pace, C.; Vajdos, F.; Fee, L.; Grimsley, G.; Gray, T., How to Measure and Predict the Molar-Absorption Coefficient of a Protein. *Protein Science* **1995,** *4* (11), 2411-2423.
22. Chakraborty, H.; Lentz, B., A Simple Method for Correction of Circular Dichroism Spectra Obtained from Membrane-Containing Samples. *Biochemistry* **2012,** *51* (5), 1005-1008.
23. Greenfield, N., Using circular dichroism spectra to estimate protein secondary structure. *Nature Protocols* **2006,** *1* (6), 2876-2890.
24. Ma, C.; Polishchuk, A. L.; Ohigashi, Y.; Stouffer, A. L.; Schön, A.; Magavern, E.; Jing, X.; Lear, J. D.; Freire, E.; Lamb, R. A.; DeGrado, W. F.; Pinto, L. H., Identification of the functional core of the influenza A virus A/M2 proton-selective ion channel. *Proc Natl Acad Sci U S A* **2009,** *106* (30), 12283-8.
25. Salom, D.; Hill, B.; Lear, J.; DeGrado, W., pH-dependent tetramerization and amantadine binding of the transmembrane helix of M2 from the influenza A virus. *Biochemistry* **2000,** *39* (46), 14160-14170.
26. Garavito, R.; Ferguson-Miller, S., Detergents as tools in membrane biochemistry. *Journal of Biological Chemistry* **2001,** *276* (35), 32403-32406.
27. Klug, C.; Feix, J.; Correia, J.; Detrich, H., Methods and applications of site-directed spin Labeling EPR Spectroscopy. *Biophysical Tools For Biologists: Vol 1 in Vitro Techniques* **2008,** *84*, 617-658.
28. Perozo, E.; Cortes, D.; Cuello, L., Three-dimensional architecture and gating mechanism of a K+ channel studied by EPR spectroscopy. *Nature Structural Biology* **1998,** *5* (6), 459-469.
29. Xu, Y.; Zhang, F.; Su, Z.; McNew, J.; Shin, Y., Hemifusion in SNARE-mediated membrane fusion. *Nature Structural & Molecular Biology* **2005,** *12* (5), 417-422.
30. Aziz, A.; Hess, J.; Budamagunta, M.; Voss, J.; Kuzin, A.; Huang, Y.; Xiao, R.; Montelione, G.; FitzGerald, P.; Hunt, J., The Structure of Vimentin Linker 1 and Rod 1B Domains Characterized by Site-directed Spin-labeling Electron Paramagnetic Resonance (SDSL-EPR) and X-ray Crystallography. *Journal of Biological Chemistry* **2012,** *287* (34), 28349-28361.
31. Nguyen, P.; Soto, C.; Polishchuk, A.; Caputo, G.; Tatko, C.; Ma, C.; Ohigashi, Y.; Pinto, L.; DeGrado, W.; Howard, K., pH-induced conformational change of the influenza M2 protein C-terminal domain. *Biochemistry* **2008,** *47* (38), 9934-9936.

32. Seddon, A.; Curnow, P.; Booth, P., Membrane proteins, lipids and detergents: not just a soap opera. *Biochimica Et Biophysica Acta-Biomembranes* **2004,** *1666* (1-2), 105-117.
33. Duong-Ly, K.; Nanda, V.; Degrad, W.; Howard, K., The conformation of the pore region of the M2 proton channel depends on lipid bilayer environment. *Protein Science* **2005,** *14* (4), 856-861.